Mineralium Deposita (2019) 54:437–458
https://doi.org/10.1007/s00126-018-0818-0

ARTICLE

The Roc Blanc orogenic Pb-Zn-Ag-Au deposit (Morocco): a product of metamorphic dehydration and CO_2 devolatilization during exhumation of the Variscan Jebilet massif

Amel El Arbaoui[1] · Mohammed Bouabdellah[2] · Amina Wafik[1] · Andreas Klügel[3] · Michel Jébrak[4] · Francesca Castorina[5,6] · Dave Lowry[7] · Pilar Lecumberri-Sanchez[8] · Abderrahim Essaifi[1] · Lhou Maacha[9]

Received: 23 October 2017 / Accepted: 8 June 2018 / Published online: 30 June 2018

Abstract

The Roc Blanc Pb-Zn-Ag ± Au vein system in the Variscan Central Jebilet massif, Morocco, is confined within the contact metamorphic aureole of S- and I-type calc-alkaline granitic stocks (327 ± 4 to 295 ± 15 Ma) along the Marrakech Shear Zone. Host rocks consist of a succession of greenschist- to amphibolite-facies metasedimentary and metavolcaniclastic rocks of Carboniferous age. The ore mineralogy is predominantly base metal and Ag-bearing sulfides and sulfosalts, intergrown with quartz and carbonates. Late-stage gold mineralization is commonly present as electrum in intimate association with all major generations of sulfide and sulfosalt minerals. Ore-related hydrothermal alteration includes silicification, sericitization, chloritization, and carbonatization. Chlorite and arsenopyrite geothermometry suggest mean temperatures of 364 and 350 °C; respectively. Calculated $\delta^{18}O_{fluid}$ values of 15 to 18‰ are consistent with metamorphic fluid sources, by which the mineralizing fluids were produced during the emplacement of granitic intrusions and subsequent devolatilization of graphitic black shale and interlayered carbonate beds. Lead and strontium isotope data constrain the source of the ore-forming components (i.e., metals and sulfur) to the enclosing host rocks. A decrease in temperature during fluid ascent and subsequent alteration-associated fluid-rock interaction resulted in the deposition of the Pb-Zn-Ag ± Au mineralization in a post-collisional extensional setting.

Keywords Variscan · Orogenic Pb-Zn-Ag-Au mineralization · REY geochemistry · Carbon, oxygen, strontium, lead isotope · Gondwana, Laurussia

Editorial handling: P. Eilu

Electronic supplementary material The online version of this article (https://doi.org/10.1007/s00126-018-0818-0) contains supplementary material, which is available to authorized users.

✉ Mohammed Bouabdellah
mbouabdellah2002@yahoo.fr

[1] Department of Geology, Cadi Ayyad University, B.P. 2390, 40000 Marrakech, Morocco

[2] Laboratoire des Gîtes Minéraux, Hydrogéologie & Environnement, Faculté des Sciences, 60000 Oujda, Morocco

[3] Fachbereich Geowissenschaften, Universität Bremen, Postfach 33 04 40, 28334 Bremen, Germany

[4] Department of Earth and Atmospheric Sciences, UQAM, 201 President Kennedy Boulevard, CP 8888 Centre Ville, Montreal, Québec H3C 3P8, Canada

[5] Dipartimento di Scienze della Terra, Università "La Sapienza", P.le Aldo Moro, 00185 Rome, Italy

[6] Instituto di Geologia Ambientale e Geoingegneria CNR, Sezione di Roma "La Sapienza", 00185 Rome, Italy

[7] Department of Earth Sciences, Royal Holloway University of London, Egham, Surrey TW20 OEX, UK

[8] Department of Earth and Atmospheric Sciences, University of Alberta, Edmonton, AB T6G 2E3, Canada

[9] Managem Group, Twin Center, Tour A, Angle Boulevards Zerktouni et Al Massira Al Khadra, B.P. 5199, 20100 Casablanca, Morocco

Introduction

Orogenic gold-silver ± base metal deposits typically occur within crustal-scale shear zones, formed over a wide range of geological settings and crustal depths and temperatures ranging from granulite to sub-greenschist facies (Groves et al. 1998; Goldfarb et al. 2005; Dubé and Gosselin 2007). Despite their great economic importance and intensive study, the genesis of this mineral deposit class remains the subject of ongoing debate regarding the potential sources of both fluids and metals. Current genetic models invoke the involvement of either metamorphic (Groves and Phillips 1987; Phillips et al. 1996), magmatic-hydrothermal (Burrows et al. 1986), or meteoric (Hagemann et al. 1994; Nesbitt and Muehlenbachs 1995) fluid sources; even mantle sources have been proposed (Groves et al. 2003; Morelli et al. 2005).

In northern Africa, as well as central and western Europe, Paleozoic inliers of the Variscan belt (Schulmann et al. 2008) host numerous economic, polymetallic vein deposits including those of "orogenic" affiliation (Boiron et al. 1990, 2003; Marignac and Cuney 1999; Bellot et al. 2003). Irrespective of origin(s), all of these deposit types are hosted by metamorphosed greenschist- to amphibolite-facies marine carbonate and clastic rocks, with the mineralized occurrences localized within intrusions or distal from them in contact metamorphic aureoles.

The Roc Blanc deposit is one of numerous Pb-Zn-Ag-Au ± Cu ± F ± Ba vein deposits that are widely distributed throughout the main Paleozoic inliers of Morocco (Margoum et al. 2015; Bouabdellah and Slack 2016), within the central part of the Jebilet orogen, ca. 20 km northwest of Marrakech (Fig. 1).

Despite its economic significance, the origin of the Roc Blanc base metal Ag-Au-rich mineralization remains controversial with regard to the source of both fluids and metals (e.g., Huvelin et al. 1978; Essarraj et al. 2017). The disagreement stems from the absence of precise constraints on the age of mineralization. Indeed, possible links between base metal Ag-Au-rich mineralization, magmatism, metamorphism, and regional tectonics remain unresolved at the district scale; importantly, the question of such genetic relationships is fundamental to successful explorations models. In this context, several conflicting hypotheses have been proposed for the genesis of Roc Blanc mineralization, with recent studies suggesting large-scale, hydrothermal circulation of basinal brines as the main ore-forming process, with the fluid system being likely related to Triassic opening of the Central Atlantic Ocean (Essarraj et al. 2017). Conversely, Huvelin (1977) suggested a Variscan age for the Roc Blanc mineralization, genetically related to emplacement of Late Variscan granitoids. Such contradictory interpretations are common for all of the hydrothermal deposits scattered throughout the Variscan belt (Marignac and Cuney 1999), and Roc Blanc appears, therefore, to be a key example to use in order to decipher this style of mineralization.

The present study is based both on field and petrographic observations of selected drill cores recovered from 13 inclined to vertical boreholes. We report here whole rock and mineral chemistry including rare earth elements plus yttrium (REY), together with C, O, Sr, and Pb isotope compositions of ore-related hydrothermal carbonates and associated Ag- and Au-bearing sulfides and sulfosalts. Gold mineralization, as yet unmined at the Roc Blanc deposit, is described herein for the first time.

In combination with observations and data reported by previous studies (Huvelin 1977; Chouhaïdi 1986; Essarraj et al. 2017), our new mineralogy, chemical, and isotopic data are used to (1) characterize the Ag- and Au-bearing mineral phases; (2) document the mineral and chemical evolution of the mineralizing fluids; (3) provide an indication of fluid source and constraints on fluid-rock interaction; and (4) evaluate the role of different fluids and ore depositional processes that operated during mineralization in the central Jebilet metallogenic province, as a framework for constructing a new genetic model.

Mining and exploration history

The Roc Blanc deposit and nearby Ag ± Au-rich prospects and showings comprise an area of about 12 × 12 km at the approximate coordinates 08° 00′ 48″ W, 31° 47′ 45″ N (Fig. 2). Early exploration in the Roc Blanc district goes back to medieval times during which Roman and Portuguese miners exploited near-surface Ag-rich oxide mineralization. The deposit was re-assessed at the beginning of the twentieth century during the French colonial period.

In 2006, Managem Group acquired the deposit and launched additional drilling and multidisciplinary geological mapping and ground-based geophysical and mineralogical studies. The deposit is now at an advanced stage of exploration. Thirteen vertical to inclined diamond drill holes covering the deposit area were drilled at 20 to 50 m spacings. Together, these investigations have delineated indicated resources estimated at > 56,000 t at 234 g/t Ag, and 200,000 t of inferred resource at 297 g/t Ag. The gold grade and resources are as yet unknown.

Regional geological setting

The central Jebilet tectono-stratigraphic block of the western Moroccan Meseta that hosts the Roc Blanc deposit (Fig. 1) consists of a > 1000-m-thick, monotonous succession of late

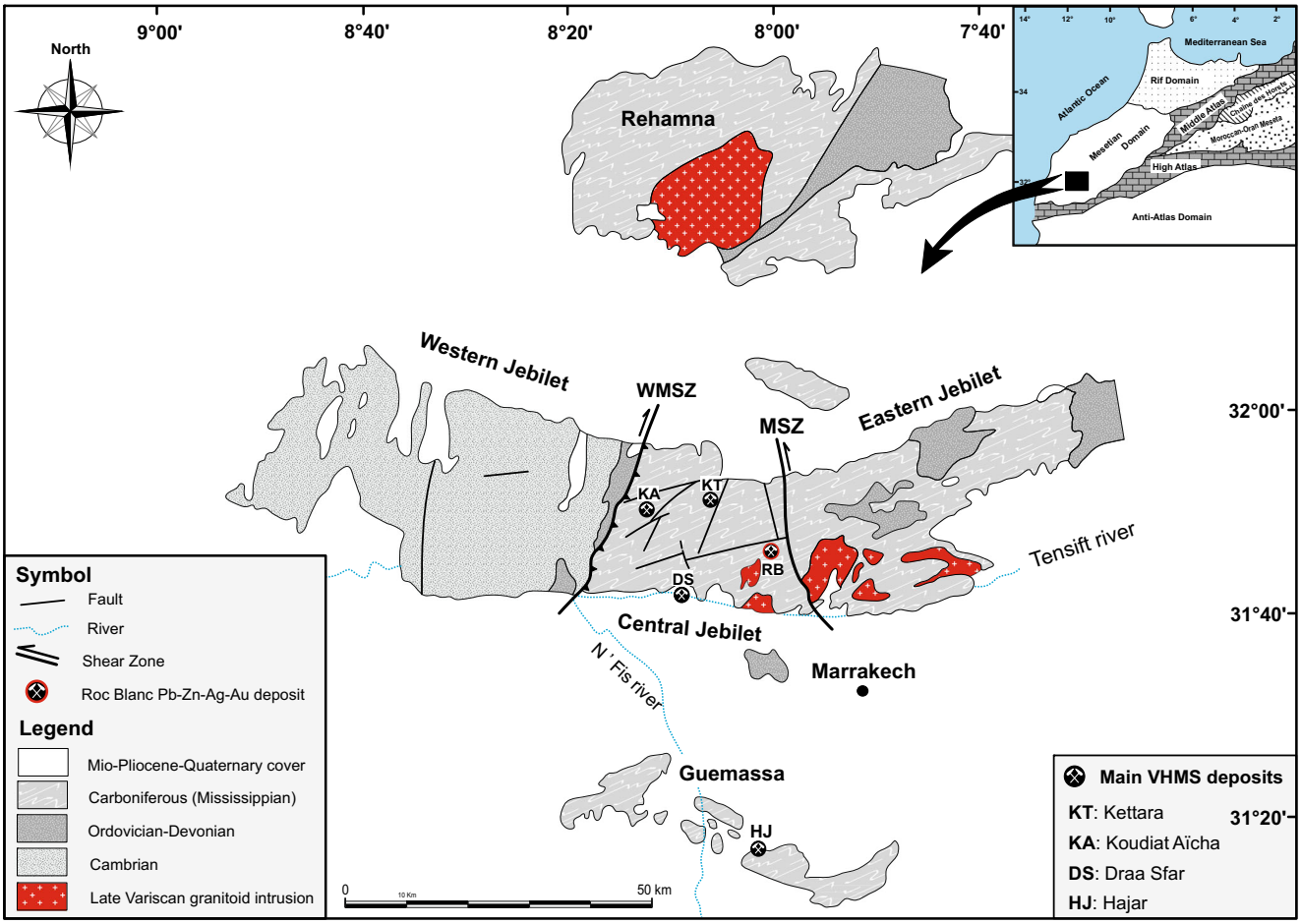

Fig. 1 Regional geologic setting of Variscan Rehamna, Jebilet, and Guemassa massifs of western Moroccan Meseta domain and locations of mined volcanic-hosted massive sulfide (VHMS) deposits at Kettara, Koudiat Aicha, Draa Sfar, and Hajar (modified from Huvelin 1977) and of Roc Blanc Pb-Zn-Ag-Au deposit. The inset shows location of central Jebilet-Guemassa VHMS province within framework of major tectono-stratigraphic domains of northern Morocco (Piqué and Michard 1989). Also shown are the Marrakech Shear Zone and Western Meseta Shear Zone, both of which delimit the trapeze-shaped block of the central Jebilet domain

Visean (Asbian) to early Serpukhovian (ca. ~331 Ma; Late Mississippian; Moreno et al. 2008), folded and metamorphosed sedimentary, volcaniclastic, and igneous rocks, both intrusive and extrusive, all of which including the intrusives are stratigraphically assigned to the Sarhlef Series (Huvelin 1977; Bordonaro 1983; Playford et al. 2008; Moreno et al. 2008). This crustal block is bordered to the west and the east by two regional-scale, graphite-rich shear zones (Fig. 1) referred to, respectively, as the NNE-trending, dextral thrust-wrench western Meseta Shear Zone (Piqué et al. 1990; Mayol and Muller 1985; Le Corre and Bouloton 1987) and the NNW–SSE sinistral wrench Marrakech Shear Zone (Lagarde and Choukroune 1982; Essaifi et al. 2001). Overall, the exposed lithologies consist predominantly of schistose organic-rich black shale with total organic carbon content averaging 0.32 wt% (Moreno et al. 2008), siltstone and sandstone with carbonate interbeds, and pyroclastic and volcanic rocks (Huvelin 1977; Bordonaro et al. 1979).

Igneous activity started at ca. 303 Ma (JICA 2003) with the emplacement of an early bimodal mafic-ultramafic to felsic suite that comprises olivine to quartz-bearing gabbro and peridotite locally intruded by a ca. 279 ± 7 Ma gabbro dike swarm. This rock package was intruded by three generations of intrusions and dike swarms including the Late Variscan granitoid stocks, and two distinct sets of leucogranite and microdiorite dikes and sheets, respectively (Figs. 2 and 3). The early intrusive rocks consist of three syntectonic, I-type or mixed S- and I-type, strongly peraluminous granitic intrusions referred to as the Bamega-Tabouchennt (22 km^2) and Bramram (0.5 km^2) stocks, and the Oulad Ouaslam (190 km^2) laccolith (Gasquet et al. 1996; Boummane and Olivier 2007; Essaifi et al. 2014), all of which are transected by a series of anastomosing, cm- to m-scale proto-mylonitic shear zones (Fig. 3). Rb-Sr ages on granite whole rock and biotite separates range from 327 ± 4 to 295 ± 15 Ma (Tisserant 1977; Mrini et al. 1992).

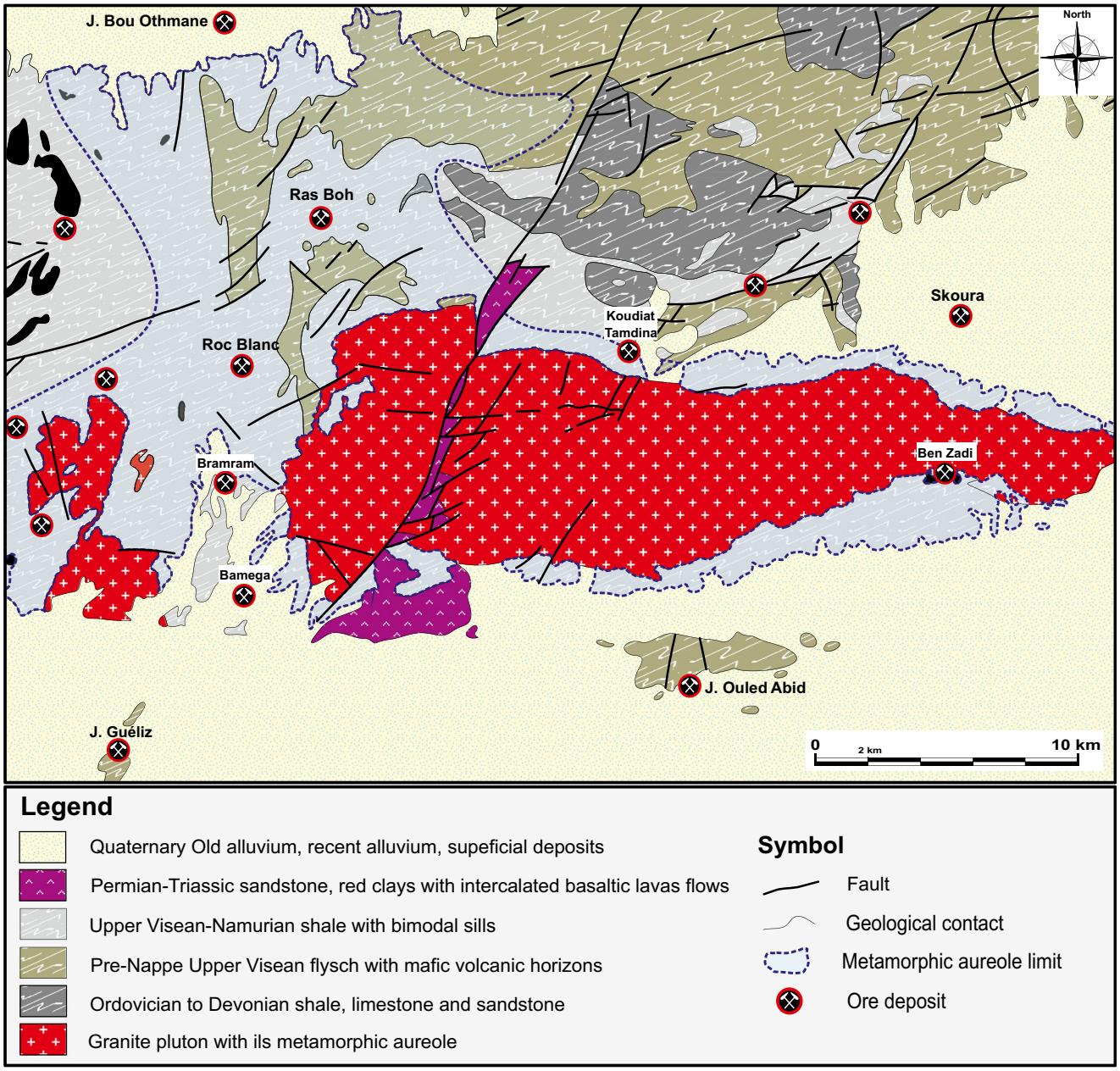

Fig. 2 Regional geologic map of Roc Blanc area showing the distribution of main lithologic units, late Variscan granitoid intrusions and associated metamorphic aureoles, major fault zones, and post-Carboniferous sedimentary rocks. Also indicated is location of principal historically mined Ag-rich deposits and prospects (modified after Huvelin et al. 1978)

The second generation of intrusions comprises a set of approximately 1-m-wide, NW-trending, sub-vertical sheet dikes of highly differentiated two mica ± tourmaline-bearing leucogranite (Fig. 3). Rb-Sr ages on whole rock average 296 ± 12 Ma (Tisserant 1977; Mrini et al. 1992).

The youngest generation of intrusive rocks consists of a swarm of up to 4-m-wide, N-S- to NE-SW-trending unmineralized and unmetamorphosed microdiorite dikes dated at ca. 255–241 ± 5 Ma (K-Ar and ^{40}K-^{40}Ar on kaersutite; Gasquet and Bouloton 1995; Youbi et al. 2001) to ca. 235 Ma (SHRIMP U–Th–Pb on zircon; Dostal et al. 2005).

Country rocks in the district have undergone polycyclic deformation and associated regional greenschist- to amphibolite-facies metamorphism (Huvelin 1977). Based on bedding-fabric-vein-fault relationships, three major deformational stages, referred to as D_1, D_2, and D_3, have been recognized (Huvelin 1977; Le Corre and Saquaque 1987; Lagarde et al. 1990; Essaifi et al. 2001; Delchini et al. 2016). Early phases of fold-and-thrust tectonics (D_1, D_2) led to the development of a series of km-scale, anticlinal and synclinal structures with sub-horizontal axes and a sub-vertical N-trending axial-planar S_1 cleavage related to D_1, followed by mesoscopic N-

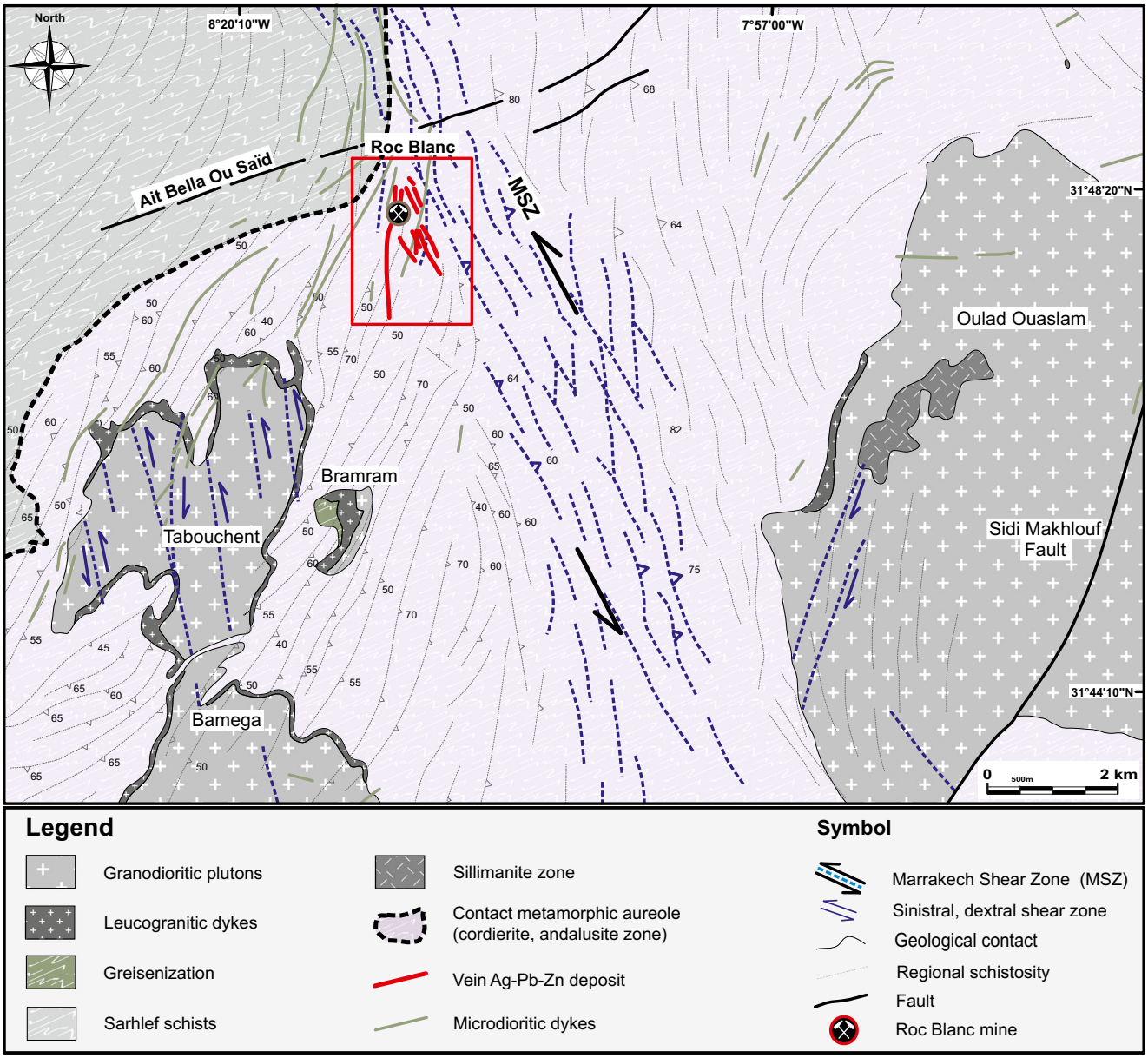

Fig. 3 Geology of the Roc Blanc Pb-Zn-Ag-Au deposit and its relationship to late Variscan granitoid intrusions and associated regional-scale Marrakech Shear Zone

trending m- to hectometric-scale folds and associated subvertical axial-planar foliation S_2 related to D_2, which has been dated to the Westphalian-Stephanian (315 ± 5 to 295 ± 5 Ma; Huvelin 1977; Huon et al. 1985; Michard et al. 2010).

D_1 was accompanied by low-grade regional metamorphism (M_1). D_2 was coeval with regional metamorphism (M_2) mostly within the greenschist facies, locally grading into amphibolite-facies conditions (Delchini et al. 2016). D_2 was either associated with, or followed by, emplacement of Late Variscan, syn- to post-kinematic granodioritic intrusions (D_3 event), which developed a mappable HT-LP metamorphic aureole (Huvelin 1977; Bordonaro 1983; El Hassani and Zahraoui 1982; Essaifi et al. 2014; Delchini et al. 2016) (Figs. 2 and 3). The resulting metamorphic mineral assemblages indicate peak thermal conditions ranging from 300 to > 500 °C and pressures of 2 ± 0.2 kb, corresponding to intrusive emplacement depths of less than 8 km (Bouloton 1992; Essaifi et al. 2001).

Overall, the ductile-brittle structures that developed during the main Variscan shortening (D_2) and associated regional metamorphism (M_2) are dominated by the first-order, sinistral and transcurrent, N-S- to NNW-SSE-trending Marrakech Shear Zone (Lagarde and Choukroune 1982). This major shear zone is locally cut by brittle ENE-trending dextral strike-slip faults (D_3), of which the Sidi Makhlouf and Aït Bella Ou Saïd faults are the most prominent (Fig. 3).

Deposit geology

The Roc Blanc deposit is in the easternmost part of the Central Jebilet within and adjacent to the N- to NNW-trending Marrakech Shear Zone, at the boundary with the Eastern Jebilet (Fig. 1). Dominant host rocks comprise a schistose and greenschist- to amphibolite-facies metamorphosed succession of Upper Visean marine organic-rich black shale with interbedded sandstone, quartzite, and carbonate.

The exploited vein system occurs within the contact aureole of the Bamega-Tabouchent intrusion along the Marrakech Shear Zone where hanging wall and footwall rocks are veined and intensely chloritized and graphitized (Figs. 3 and 4). Pb-Zn-Ag-Au mineralization consists of massive, open-space fillings of a complex, anastomosing network of transtensional, mostly NNW- to NNE-trending, sub-vertical veins, veinlets, and en echelon tension gashes.

Seven principal, subparallel, and steeply dipping mineralized veins, referred to as V_1 through V_7, were exploited (Fig. 4). Individual veins consist of one or more discontinuously mineralized shear segments. Geometric and chemical characteristics of these veins are summarized in Table 1. Among all veins that constitute the Roc Blanc deposit, V_5 is historically and economically the most significant, accounting for nearly all of the extracted ore from the mine. The orebodies contain 160 to 1500 g/t Ag (locally up to 2800 g/t), 1.2 to 2.8 wt% Pb, and 1.2 to 2.5 wt% Zn (up to 3.35 wt%). Diamond drill holes implemented by Managem Group intersected V_5 at different levels (down to 800 m below surface), where hydrothermally altered and veined, organic-rich black shale host significant Ag grades (1533 g/t over 1.7 m; Fig. 5a, b), adjacent to the Marrakech Shear Zone.

Overall, the mineralized veins extend laterally for as much as ~ 2 km along strike, are spaced 50 to > 100 m apart, dip between 35° and 65° to the east, vary in thickness from several cm up to 2 m, display similar morphological and textural features, and exhibit sharp margins with host rocks. Known vertical extents of mineralization are greater than 800 m. The veins pinch (Fig. 6a) and bifurcate into smaller veinlets and undulate along strike and down dip. Most vein margins are brecciated and cemented by hydrothermal Ca-Fe-Mg carbonates and drusy or comb-textured quartz (Fig. 6b). A set of post-mineralization faults truncates the veins with offsets of several cm.

Laminated (Fig. 6c), cockade (Fig. 6d), comb, breccia, and crack-and-seal textures suggest episodic mechanisms were important for vein formation. Pervasive hydrothermal alteration has affected, to varying degrees, all of the country rocks, particularly those adjacent to the mineralized structures that overprint the metamorphic assemblage. Alteration halos range from cm-wide selvages to 3-m-wide zones that envelope the veins. The alteration halos comprise variable proportions of white sericite-muscovite (Fig. 6e), chlorite (Fig. 6e), quartz, hydrothermal Ca-Fe-Mg carbonates (ferroan dolomite, ankerite-siderite, calcite) (Fig. 6g), tourmaline (Fig. 6h), albite, rutile, ilmenite, magnetite, and sulfide minerals.

Sampling and analytical methods

The samples used in this study are half-core specimens from 13 vertical drill holes (Fig. 4) that intersected the entire thickness of the major veins, surface outcrops, and underground exposures.

Silicate, carbonate, sulfosalt, and sulfide minerals were characterized at the University of Cadi Ayyad of Marrakech and REMINEX Research Center of Managem Group (Morocco) using a Philips XL30 environmental scanning electron microscope, coupled to an Oxford Instruments energy-dispersive X-ray analysis system (SEM-EDS).

Major element (Ca, Mg, Fe, Mn) and trace element contents of Fe-Mg-Ca carbonates were measured by laser-ablation inductively coupled plasma-mass spectrometry (LA-ICP-MS) at the Department of Geosciences, University of Bremen (Germany). Ca was determined from the Ca, Mg, Fe, and Mn analyses by normalizing (Ca, Mg, Fe, Mn)CO_3 to 100 wt%. Details of the system design, laser characteristics, and experimental conditions are described in Jochum et al. (2012) and Margoum et al. (2015).

Chemical compositions of major sulfide and sulfosalt minerals were determined using a JEOL JXA-8200 electron probe microanalyzer (EPMA) equipped with wavelength and energy-dispersive spectrometers (WDS and EDS) at the Department of Earth Sciences, University of Milan (Italy), following the procedure of in Sessa et al. (2017).

Carbon and oxygen isotope analyses of carbonate separates were carried out at Royal Holloway University of London (UK) following the method described in Bouabdellah et al. (2015). External precision (1σ) on multiple analyses of the carbonate standards during the sample analysis period was better than ± 0.05 ‰ for $\delta^{13}C$, and ± 0.1 ‰ for $\delta^{18}O$ after correction for scale compression. Isotopic data are reported relative to Standard Mean Ocean Water (V-SMOW) for oxygen and PeeDee Belemnite (V-PDB) for carbon.

Strontium isotope analyses were performed at the IGAG-CNR, Dipartimento di Scienze della Terra, University of Rome 'La Sapienza' using a FINNIGAN MAT 262RPQ multicollector mass spectrometer with Re single filaments in static mode. Repeated analyses of standards gave averages and errors expressed as two-standard deviations (2σ), as

Fig. 4 Property-scale geology map of Roc Blanc deposit showing the distribution of surrounding host rock lithologies, seven veins that contain Pb-Zn-Ag-Au resources and their relationship to the ca. 255–235 Ma dioritic dike swarm, and the Marrakech Shear Zone and associated major fault structures

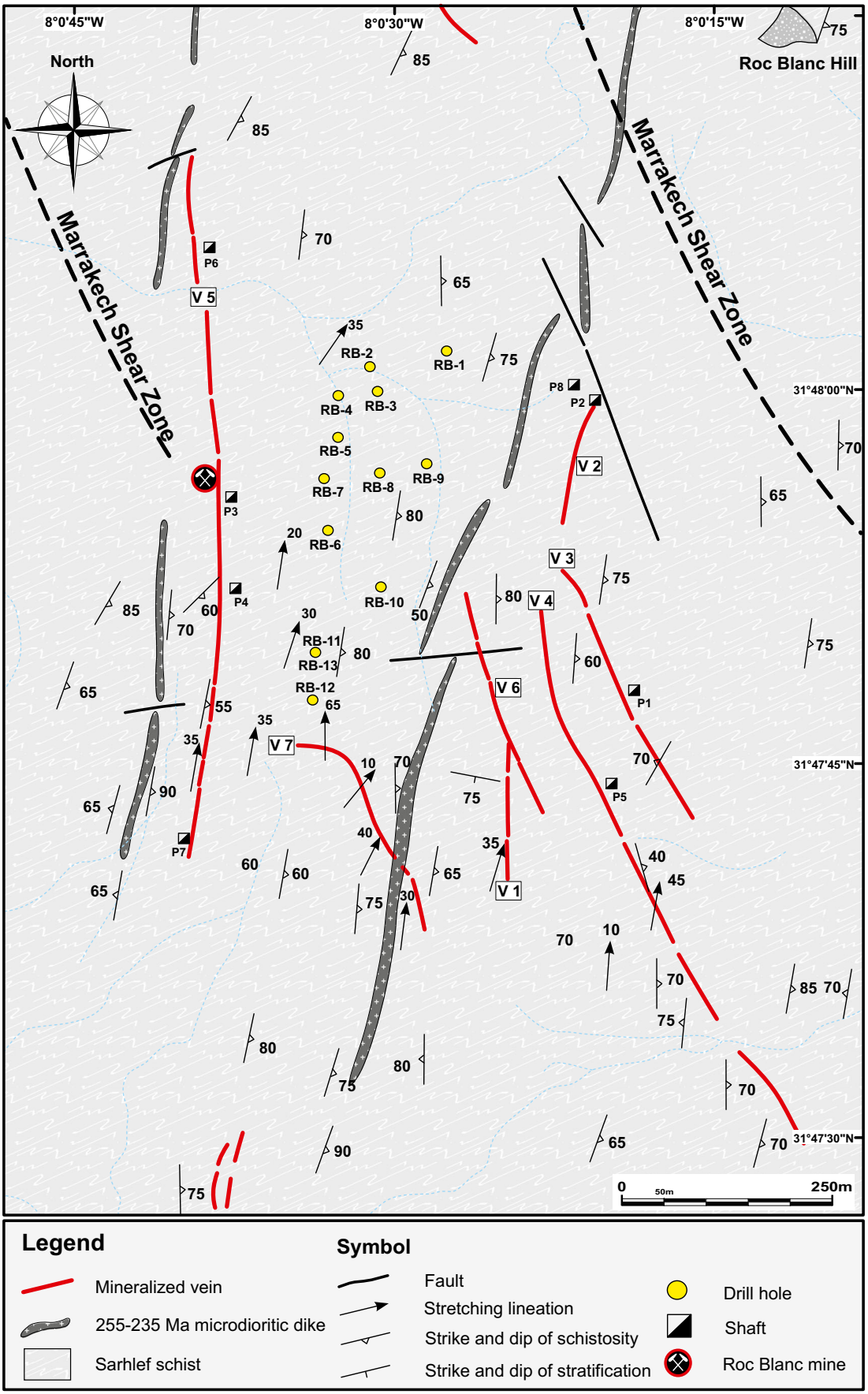
8°0'45"W
8°0'30"W
8°0'15"W
North
Roc Blanc Hill
Marrakech Shear Zone
Marrakech Shear Zone
31°48'00"N
31°47'45"N
31°47'30"N
RB-1
RB-2
RB-3
RB-4
RB-5
RB-6
RB-7
RB-8
RB-9
RB-10
RB-11
RB-12
RB-13
V 1
V 2
V 3
V 4
V 5
V 6
V 7
P1
P2
P3
P4
P5
P6
P7
P8
0
50m
250m
Legend
Mineralized vein
255-235 Ma microdioritic dike
Sarhlef schist
Symbol
Fault
Stretching lineation
Strike and dip of schistosity
Strike and dip of stratification
Drill hole
Shaft
Roc Blanc mine

Table 1 Summary of the geometrical characteristics and metal contents of major Ag-Pb-Zn veins in the Roc Blanc deposit

Vein no.	Strike	Dip	Strike length (m)	Width (m)	Ag (ppm)	Pb (wt%)	Zn (wt%)	Ore mineralogy
V1	10°~15°	45°~55°	170	0.2~0.5	Unknown	Unknown	Unknown	Sp-Gn-Ag-Ttr-Po-Py-Asp
V2	10°~15°	45°~50°	170	0.3~0.6	260	1.52	1.2	Apy-Py-Gn-Ag-Ttr
V3	330°~335°	70°~75°	300	0.2~0.7	1500	1.68	2.52	Gn-Ag-Ttr-Sp-Py-Asp
V4	330°~335°	65°~70°	600	0.3~0.75	1500	2.82	1.54	Gn-Ag-Ttr-Sp-Py-Asp
V5	10°~15°	45°~55°	2.000	0.4~0.8	2800 (297)[a]	1.2 (1.65)[a]	3.35 (2.12)[a]	Gn-Sp-Py-Apy-Ag-Ttr-Cpy-Po
V6	330°~335°	65°~90°	300	0.2~0.5	1450	Unknown	Unknown	Sp-Gn-Ag-Ttr-Po-Py-Cpy
V7	330°~340°	65°~80°	300	0.2~0.5	160	Unknown	Unknown	Sp-Py-Po-Gn-Ag-Ttr

Sp sphalerite, *Gn* galena, *Py* pyrite, *Asp* arsenopyrite, *Po* pyrrhotite, *Cpy* chalcopyrite, *Ag-Ttr* argentiferous tetrahedrite

[a] 2012 updated data from Managem Group Mining Company

follows: NBS 987, $^{87}Sr/^{86}Sr = 0.710231 \pm 13$ ($n = 10$), $^{86}Sr/^{88}Sr$ normalized to 0.1194. Total procedural blanks were below 2 ng of Sr.

Lead isotopic compositions of galena separates were determined at the GEOTOP Radiogenic Isotope Laboratories at the Université du Québec à Montréal (UQAM) following the methods outlined by Conliffe et al. (2013). Data are reported as $^{206}Pb/^{204}Pb$, $^{207}Pb/^{204}Pb$, and $^{208}Pb/^{204}Pb$ with an analytical uncertainty of 0.05% amu^{-1} at the 1 σ level (Moritz and Malo 1996).

Vein mineralogy

All mineralized veins display similar mineral assemblages but proportions of base metal sulfides relative to other minerals vary among the veins. Antimony sulfosalts and Fe-Ti oxides (magnetite and rutile) are also present. Alteration gangue minerals consist predominantly of quartz, hydrothermal Ca-Fe-Mg carbonates, sericite, and chlorite. Sulfides generally constitute less than 15 vol% of the veins, although higher concentrations (up to ~ 30 vol%) are observed in high-grade ore.

Sulfide and antimony sulfosalt minerals

Sulfide minerals are, in decreasing order of abundance, pyrite, sphalerite, and galena with minor chalcopyrite, arsenopyrite, and pyrrhotite. Other sulfide and antimony sulfosalt minerals include freibergite-argentotennantite, boulangerite, ullmannite, and meneghinite.

Pyrite occurs as annealed aggregates up to several cm in diameter that consist of pyritohedral crystals (< 200 μm), and massive aggregates in thicker (> 5 cm) carbonate-rich veins. Pyrite also forms disseminated euhedral to subhedral grains (Fig. 7a) in altered wall rocks close to the mineralized veins. Irrespective of morphology and paragenetic position, pyrite shows little variation in chemistry and approaches the ideal stoichiometric formula FeS_2 (Electronic Supplementary Materials (ESM) 1). Minor elements in pyrite include As, Zn, and Cu in concentrations of 0.1 to 1.5, 0.01 to 0.26, and 0.01 to 0.08 wt%, respectively. Overall, these representative compositions plot within the field of orogenic pyrite as defined by Deditius et al. (2014) (Fig. 8).

Sphalerite occurs as disseminated dark brown to light brown (Fig. 7a), medium to coarse grains (up to several cm) or as massive crystalline aggregates that cement clasts in breccias and fill open spaces within the veins. EPMA analyses indicate Fe contents from 2.7 to 6.4 wt%. Abundances of trace elements such as Cd, As, Hg, Ni, Co, Cu, Pb, Ag, and Au are low, with most concentrations fringing detection limits (ESM 1).

Morphology of galena range from disseminated, fine- to coarse-grained crystals, to anhedral masses (Fig. 7b), to massive bands several cm thick, to elongate radiating crystals filling veins. Irrespective of habit, galena crystals are compositionally homogeneous and lack enrichment in trace elements (ESM 1). Although galena is paragenetically related to silver minerals, most analyses of galena in this study reveal Ag contents of < 0.5 wt% (ESM 1).

Chalcopyrite forms massive mono- or polymineral aggregates commonly intergrown with pyrrhotite, galena, and iron-rich sphalerite, or as anhedral masses filling microfractures within pyrrhotite with little or no replacement. Chalcopyrite may also occur as fine-grained inclusions ("chalcopyrite disease"; Barton Jr 1978; Barton Jr and Bethke 1987) within iron-rich sphalerite (Fig. 7c). EPMA analyses indicate an homogenous composition close to the ideal formula $CuFeS_2$ (ESM 1).

Arsenopyrite is rare and forms fine-grained (2–70 μm) rhombic and subhedral inclusions (Fig. 7b) or intergrowths with pyrite and iron-rich sphalerite. Locally, arsenopyrite is fractured or brecciated, with the microfractures healed by sphalerite, galena, and argentotennantite. EPMA analyses reveal an homogenous composition close to stoichiometric FeAsS with As, Fe, and S contents of 42–43, 35–37, and 21–23 wt%, respectively (ESM 1). Using the fS_2-buffered

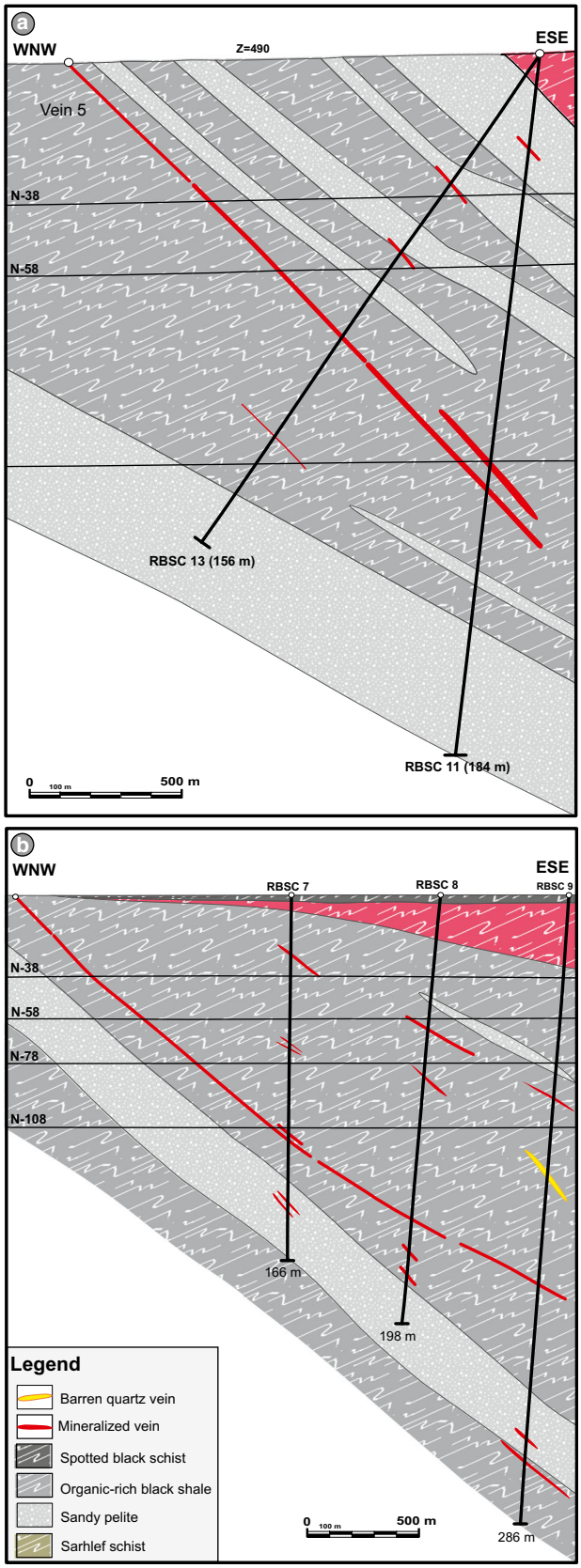

Fig. 5 Representative WNW-ESE cross section through the V_5 exploration line showing distribution and morphology of veins, surrounding lithologies, and exploration levels

arsenopyrite-pyrite-pyrrhotite equilibrium (Barton Jr and Skinner 1979; Pokrovski et al. 2002), this compositional range suggests a mean crystallization temperature of 350 ± 20 °C.

Pyrrhotite occurs either as anhedral granular aggregates (0.1–10 mm) or as inclusions in pyrite in association with chalcopyrite. It also fills fractures in pyrite associated with the second generation of hydrothermal Ca-Fe-Mg carbonates, Fe-rich sphalerite, galena, and chalcopyrite, all of which are embedded in a gangue quartz, chlorite, muscovite, and tourmaline. EPMA analyses of the pyrrhotite show an homogenous composition close to Fe_{1-x} S (ESM 1).

Also present in the veins are rare occurrences of boulangerite ($Pb_5Sb_4S_{11}$), meneghinite ($Pb_{13}CuSb_7S_{24}$), and ullmanite (NiSbS) that commonly form microscopic, anhedral to euhedral inclusions in pyrite, galena, chalcopyrite, argentotennantite, and pyrargyrite.

Silver minerals

Silver minerals are abundant in all major veins and include freibergite-argentotennantite, owyheeite, diaphorite, pyrargyrite, polybasite, stephanite, miargyrite, argentite, argentopyrite, and native silver. Characteristic are massive aggregates within sphalerite, galena, and chalcopyrite, interstitial grains between sulfides and quartz and/or ore-related hydrothermal Ca-Fe-Mg carbonates, or irregular veinlets or stringers in sphalerite, tetrahedrite, and chalcopyrite. EPMA analyses and related calculated structural formulae of the major Ag-bearing minerals are presented in ESM 1.

Argentiferous tetrahedrite of the freibergite-tennantite series is by far the most abundant silver mineral (Fig. 7a, b). It commonly occurs as (1) replacements of galena; (2) 0.1- to 20-mm anhedral grains; (3) massive aggregates intergrown with sphalerite, galena, chalcopyrite, pyrite, polybasite, pyrargyrite, and boulangerite; and (4) infillings of fractures. Argentiferous tetrahedrite crystals show a large range in Ag (29.5–33.4 wt%), Sb (14.51–26.32 wt%), and As (0.07 to 3.15 wt%) contents (ESM 1), allowing their classification as freibergite and argentotennantite. Minor components include Zn, Fe, and As at 1.0 to 2.4, 3.7 to 5.5, and 0.1 to 3.2 wt%, respectively.

Pyrargyrite forms interstitial stringers between pyrite, galena, and polybasite, anhedral crystals (< 0, 1 mm) in tetrahedrite intergrown with miargyrite and argentite, and euhedral crystals lining vugs within quartz and ore-related hydrothermal Ca-Fe-Mg carbonates. Pyrargyrite grains contain 59 to 60 wt% Ag, 20 to 22 wt% Sb, and > 0.1 to 1.4 wt% Cu (ESM 1).

Polybasite occurs as anhedral crystals of varying size (< 0.01 mm) or inclusions in, or grains adjacent to, argentotennantite, pyrargyrite, and galena. Silver contents range from 68.3 to 74.8 wt%; Cu and Sb are in the range of 1.8 to

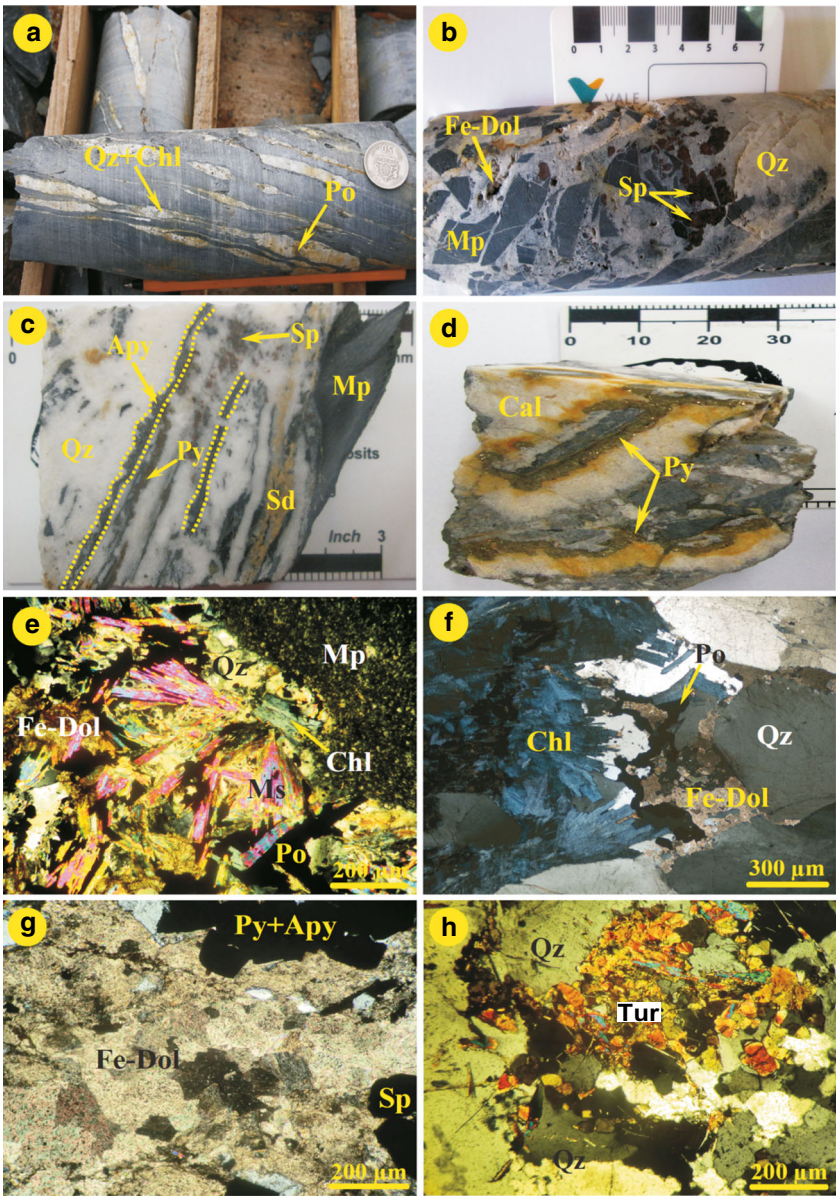

Fig. 6 Representative photographs of drill cores (**a**–**d**) and transmitted-light photomicrographs (**e**–**h**) illustrating modes of occurrence, textures, alteration, and gangue mineral assemblages in Roc Blanc Pb-Zn-Ag-Au deposit. **a** Pinch-and-swell geometry of quartz-chlorite vein. Coin diameter = 2 cm. **b** Typical example of quartz-carbonate-cemented hydrothermal ore-bearing breccia. **c** Typical banded vein with parallel quartz and siderite ribbons, and subsidiary sulfides and siderite. **d** Cockade texture developed in brecciated quartz-carbonate-pyrite vein. **e** Radiating muscovite and chlorite crystals with ferroan dolomite and pyrrhotite; crossed polars. **f** Chlorite and pyrrhotite from early sulfide stage in quartz and ferroan dolomite vein; crossed polars. **g** Pyrite, arsenopyrite, and sphalerite closely associated with ore-related ferraon dolomite; crossed polars. **h** Metamorphic-hydrothermal tourmaline aggregates closely associated with quartz, crossed polars. Abbreviation: Apy = arsenopyrite, Chl = chlorite, Fe-dol = ferroan dolomite, Qz = quartz, Mp = metapelite, Ms = muscovite, Po = pyrrhotite, Py = pyrite, Sd = siderite, Sp = sphalerite, Tur = tourmaline

7.3 and 6.1 to 10.6 wt%, respectively. Abundances of As are very low with most concentrations near detection limits (ESM 1).

Owyheeite, a sulfo-antimonide ($Pb_{10}Ag_3Sb_{11}S_{28}$) mineral, is widespread and abundant in the vein system. It forms euhedral to sub-euhedral crystals with grain sizes up to several mm and inclusions in, or borders on, boulangerite, sphalerite, and argentotennantite. Locally, owyheeite is replaced by andorite. Owyheeite contains 44 to 47 wt% Pb, 28.6 to 30.3 wt% Sb, and 5.9 to 7.0 wt% Ag (ESM 1). Minor components include Cu and As at 0.2 to 0.5 and 0.1 to 0.3 wt%, respectively.

Stephanite forms thin selvages or overgrowths coating native silver and in places as submicroscopic inclusions within galena and argentiferous tetrahedrite (Fig. 7a, b). Silver contents range from 61.2 to 63.8 wt% (ESM 1). Minor components include Pb, Zn, and Cu at ~0.1 to 0.5, 0.2 to 0.3, and ~0.1 to 1.2 wt%, respectively.

Diaphorite ($Ag_3Pb_2Sb_3S_8$) occurs as polysynthetic, twinned, euhedral to sub-euhedral crystals with grain sizes up to 20 mm in contact with sphalerite (Fig. 7b), miargyrite, and pyrargyrite. Diaphorite also is present as drop-like inclusions in galena and freibergite. It contains 23.2 to 24.2 wt% Ag, 28.7 to 30.1 wt% Pb, and 26.6 to 28.8 wt% Sb (ESM 1).

Argentite forms rare submicroscopic isolated inclusions within galena (Fig. 7d) and in argentotetrahedrite with silver contents averaging 87 wt% (ESM 1).

Accessory Ag-bearing minerals include miargyrite ($AgSbS_2$; 37.1–39.3 wt% Ag), and argentopyrite (34.9–35.2 wt% Ag), both of which occur as submicroscopic grains within major sulfides and sulfosalts (Table 2).

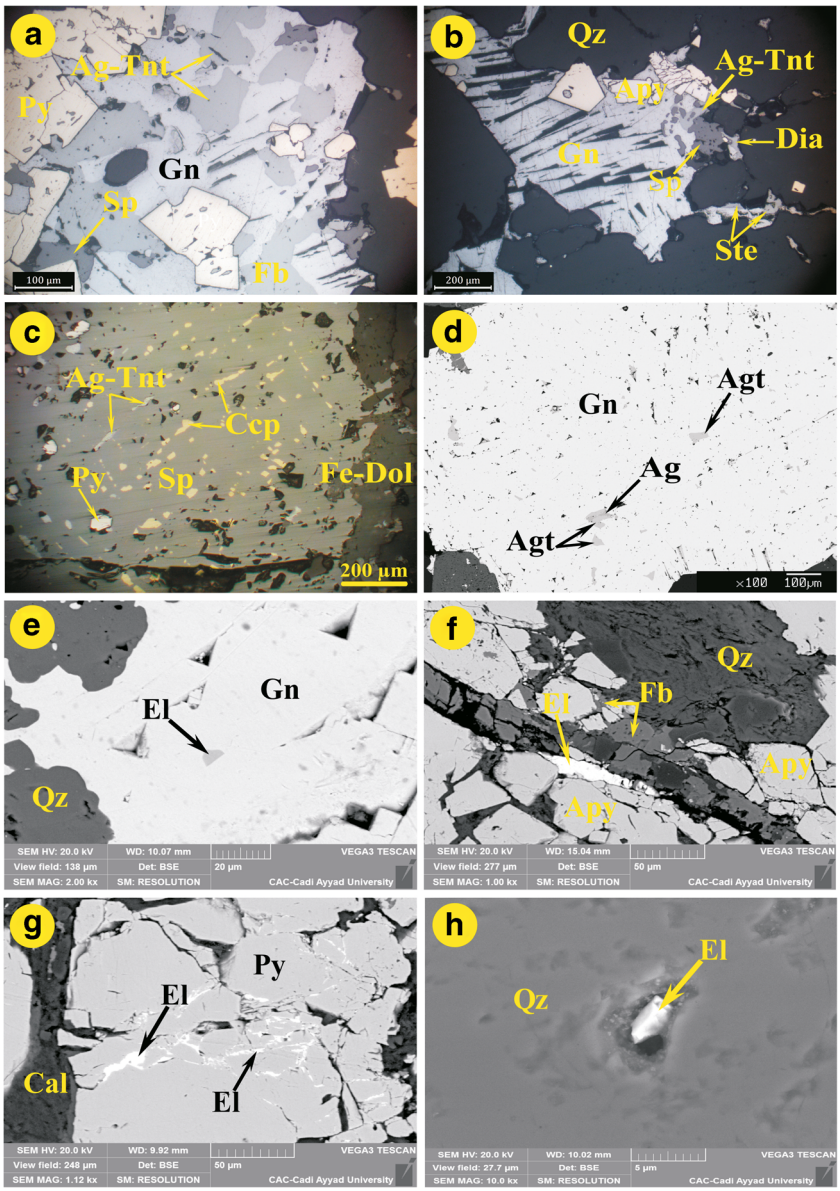

Fig. 7 Representative reflected and plane-polarized light photomicrographs (**a**–**d**) and back-scattered electron images (**e**–**h**) showing mineral assemblages and ore textures of base metal and Ag- and Au-bearing sulfides and sulfosalts from Roc Blanc Pb-Zn-Ag-Au deposit. **a** Galena (Gn) intergrown with argentotennantite (Ag-Tnt), sphalerite (Sp), and diaphorite (Dia) overprinted by stephanite (Ste) in quartz vein. **b** Argentotennantite (Ag-Tnt) associated with sphalerite (Sp), pyrite (Py), and freibergite (Fb). **c** Anhedral sphalerite (Sp) with chalcopyrite (Ccp) and argentotennantite (Ag-Tnt) exsolution in carbonate-sulfide vein with void space filled by pyrite (Py). **d** Inclusions of argentite (Agt) and native silver (Ag) within galena crystal. **e** Inclusion of electrum (El) in galena (Gn). **f** Intergrowths of arsenopyrite (Apy), freibergite (Fb), and quartz (Qz) with electrum (El) filling remaining space. **g** Native gold healing microcracks within pyrite. **h** Electrum (El) filling void within quartz (Qz)

Native silver commonly is closely intergrown with galena or argentite (Fig. 7d). It is also observed as "wire" grains cutting or replacing galena, freibergite, and chalcopyrite, or filling open spaces. SEM-EDS spot analyses reveal up to 10 wt% Au.

Textural relationships indicate a paragenetic sequence for the silver minerals, from early to late, consisting of argentotennantite-freibergite series (29.5–31.8 wt% Ag) → miargyrite (37.1–39.3 wt% Ag) → pyrargyrite (59–60 wt% Ag) → stephanite (61.2–63.8 wt% Ag) → polybasite (68.3–74.8 wt% Ag) → argentite (86–87 wt% Ag) → native silver (> 90 wt% Ag). This succession indicates that a correlation exists between the paragenetic position of a given sulfide-sulfosalt mineral. Importantly, there is a trend of increasing Ag content from early to late Ag-rich minerals.

Gold minerals

Gold, commonly forming electrum, occurs in intimate association with all major generations of sulfide and sulfosalt minerals related to the main vein filling. Nearly all of the gold (> 95%) forms subhedral to anhedral inclusions and blebs (Fig. 7e), typically along grain boundaries (Fig. 7f), and fillings of deformation cracks, veinlets, and microfractures (Fig. 7g). The remaining gold (< 5%) occurs in quartz-ferroan dolomite-ankerite veins (Fig. 7h). Grain sizes are typically 5 to 30 µm and may reach 110 µm. SEM-EDS analyses indicate that the gold contain 53–88 wt% Au and 12–47 wt% Ag, together with trace amounts of Sb (up to 1 wt%). Textural relationships suggest that gold mineralization took place during at least two distinct events, during and after deposition of

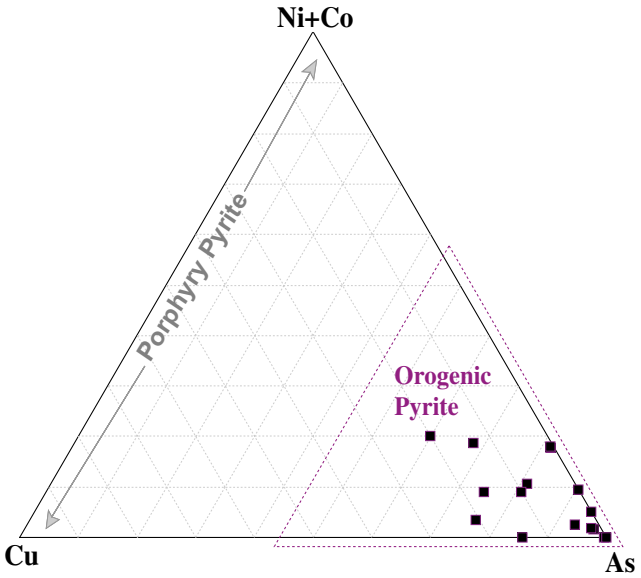

Fig. 8 Ternary discrimination plot showing compositional variations of pyrite from Roc Blanc deposit in term of (Ni + Co)-Cu-As end-member components with orogenic pyrite field of Deditius et al. (2014)

the sulfides and sulfosalts. The early gold (Au-1) forms rounded inclusions within sulfide-sulfosalt crystals, whereas the second phase of gold (Au-2) forms along fractures and at grain boundaries (Fig. 7f, g) where the sulfide and sulfosalt hosts were brecciated, suggesting that Au-2 at least locally postdates deposition of the host minerals.

Gangue minerals

Quartz is by far the predominant vein filling constituent (> 80 vol%) and at least four distinct generations of translucent to milky white quartz are recognized. Early quartz veins are rarely recognized by cross-cutting relationships but more commonly as quartz-rich lenses and porphyroblasts dispersed within graphite-rich schistose black shale. The second generation occurs in the outer part of the veins and is intergrown with muscovite and, to a lesser extent, chlorite but is typically replaced by pyrrhotite, iron-rich sphalerite, and chalcopyrite. The third generation of quartz consists predominantly of milky, white, coarse-grained, euhedral to subhedral, interlocking, sutured, polygonized or strained quartz grains intergrown with siderite, ferroan dolomite-ankerite, and calcite, coexisting with galena, sphalerite, pyrite, arsenopyrite, and silver-bearing minerals. The late quartz generation forms drusy or comb-textured grains without associated sulfide, sulfosalt, or precious-metal minerals and is termed post-ore barren quartz.

Hydrothermal Ca-Fe-Mg carbonates occur widely and occupy an average volume in the veins of 5% reaching locally up to 25 vol%. The carbonates dominantly form (1) white to yellowish, euhedral to anhedral, medium to coarse grains; (2) massive aggregates mostly intergrown with galena, sphalerite, chalcopyrite, and quartz; and (3) filling microfractures. SEM-EDS, EPMA, and LA-ICP-MS analyses (ESM 2) indicate that the analyzed carbonates fall into three main compositional groups: calcite, Mg-rich siderite (sideroplesite to pistomesite, hereafter referred to as siderite), and ferroan dolomite to ankerite (Fig. 9).

Based on composition and paragenetic position, three generations of hydrothermal Ca-Fe-Mg carbonates are observed. The early variety carbonate-1 forms euhedral crystals up to 1 cm in size, forming ribbons at selvages of the veins. The second ore-stage hydrothermal carbonate-2 makes up the largest volume (up to 50%) of carbonate cements and apparently is contemporaneous with the main ore stage of vein filling (Fig. 10). It occurs as patches and curved "saddle" crystals surrounding the veins and filling secondary porosity within the veins, in fractures, and to a lesser extent solution breccias; it also replaces the surrounding matrix. Carbonate-2 is associated with sphalerite, galena, and chalcopyrite, and locally with pyrrhotite, pyrite, or Ag-Au-bearing minerals. Late post-ore carbonate-3 postdates ore-stage sulfides and sulfosalts, commonly occurring in the center of veins only as open-space fillings.

Chlorite displays a wide spectrum of textures and mineral associations, particularly as a green groundmass, fibrous radial aggregates aligned parallel to foliation planes, or structurally controlled fracture fillings in association with pyrite, quartz, and Ca-Fe-Mg carbonates surrounding individual veins. EPMA analyses (ESM 3) show homogenous ripidolitic compositions (MgO = 4–10 wt%; Fe/[Fe + Mg] = 0.63–0.84; Al^{IV} = 2.68–2.86 atoms per formula unit) according to Hey (1954) (ESM 4A). Chlorite geothermometry, using the approach of Cathelineau and Nieva (1985) and Kranidiotis and MaClean (1987), indicates formation temperatures between 352 and 382 °C and averaging 364 °C (ESM 4B), which are consistently higher than the temperatures inferred from fluid inclusion data (Essarraj et al. 2017).

Vein paragenetic sequence

An idealized sequence of mineral deposition, drawn from cross-cutting relationship of veins, alteration, and ore-mineral assemblages, together with textural observations, shows the existence of three successive and overlapping stages of mineralization (Fig. 10). Each of these stages is separated by episodes of intense shearing and brecciation and may be correlated at the scale of the vein field.

The early, uneconomic stage I, which predated major shearing (D_2), consists of fault-controlled, pyrite-arsenopyrite-pyrrhotite-quartz veins and is characterized by the deposition of carbonate-1 (mainly siderite) along vein selvages.

Later main vein filling stage II formed predominantly during D_2–D_3 shearing and fracturing events, and accounts for all

Table 2 Carbon, oxygen, and strontium isotope compositions of ore-related hydrothermal Ca-Fe-Mg carbonates from major veins of Roc Blanc Pb-Zn-Ag-Au deposit compared to those of potential metal source rocks (i.e., organic-rich black shale, rhyodacite, late Variscan granite)

Sample No.	Mineral/Rock	δ^{18}OV-SMOW (‰)	δ^{13}CV-PDB (‰)	Rb (ppm)	Sr (ppm)	$^{87}Sr/^{86}Sr \pm 2s$
Carbonate separate						
RB 1	Ferroan dolomite	23.3	-6.8		60	0.714535 ± 10
RB 2	Ferroan dolomite	22.1	-7.0			
RB 6	Ferroan dolomite	22.9	-7.8		138	0.710157± 22
RB 9	Ferroan dolomite	22.6	-7.5		149	0.708043± 11
RB 17	Ferroan dolomite	22.4	-6.8		67	0.713051 ± 19
RB 18	Ferroan dolomite	22.8	-6.9		133	0.709368 ± 14
RB 19	Ferroan dolomite	22.7	-6.8			
RB 23	Ferroan dolomite	22.6	-7.2		133	0.709612 ± 12
RB 28	Ferroan dolomite	22.3	-7.5			
RB 16	Ferroan dolomite				132	0.712714 ± 11
RB 29	Ferroan dolomite				39	0.710435 ± 12
RB 3	Siderite	21.7	-6.1		120	0.714421 ± 12
RB 5	Siderite	22.2	-7.0			
RB 11	Siderite	17.2	-10.6			
RB 14	Siderite	15.8	-9.1		139	0.715961 ± 20
RB 15	Siderite	23.0	-6.6		124	0.714474 ± 17
RB 21	Siderite	22.0	-5.0		144	0.715088 ± 12
RB 24	Siderite	21.3	-7.4		125	0.714052 ±21
RB 25	Siderite	23.2	-7.6		105	0.714388 ±10
RB 4	Calcite	19.5	-7.9		427	0.714837 ± 20
RB 7	Calcite	19.3	-8.3		401	0.714987 ± 11
RB 8	Calcite	21.5	-6.9		148	0.715230 ± 9
RB 10	Calcite	19.4	-7.9			
RB 13	Calcite	24.4	-6.1		392	0.716049 ± 9
RB 26	Calcite	20.3	-8.9		124	0.713888 ± 10
Whole-rock						
JC 1	Visean Organic-rich black shale			138	216	0.737615 ± 9
JC 2	Visean silty limestone			108	65	0.711681 ± 8
JC 3	Visean silty limestone			132	80	0.710535 ± 9
JC 7	Visean porpyritic rhyodacite			23	300	0.717088 ± 7

of the exploited ores in the Roc Blanc deposit. It consists of sequentially deposited sphalerite, galena, chalcopyrite, and Ag- and Au-bearing sulfide and sulfosalt minerals, together with ore-stage hydrothermal Ca-Fe-Mg carbonate-2. Minerals of this paragenesis are spatially associated with distinctive and strongly silicic, sericitic, carbonatitic, and locally chloritic alteration zones. Native gold occurs within late structures. Based on the amounts of base metal sulfides relative to Ag- and Au-bearing sulfide-sulfosalt-antimony mineral assemblages, three sub-stages of alteration and mineralization are distinguished within stage II. These are referred to as base metal-rich, Ag-rich, and Au-rich sub-stages (Fig. 10).

The latest stage, termed post-ore barren stage III, occurs in calcite or quartz veins, or as late fillings within the oldest stages as linings of the remaining open spaces.

Supergene effects are minimal. The main oxides include goethite, hematite, and manganese oxides, mainly as fracture coatings. There is no obvious supergene enrichment of hypogene grades.

Analytical results

Trace element and REY compositions of ore-related Ca-Fe-Mg carbonates

Similar to major element compositions, trace element abundances of the different types of ore-related hydrothermal Ca-Fe-Mg carbonates are highly variable (ESM 2). With respect to REY, ankerite and ferroan dolomite separates show, on

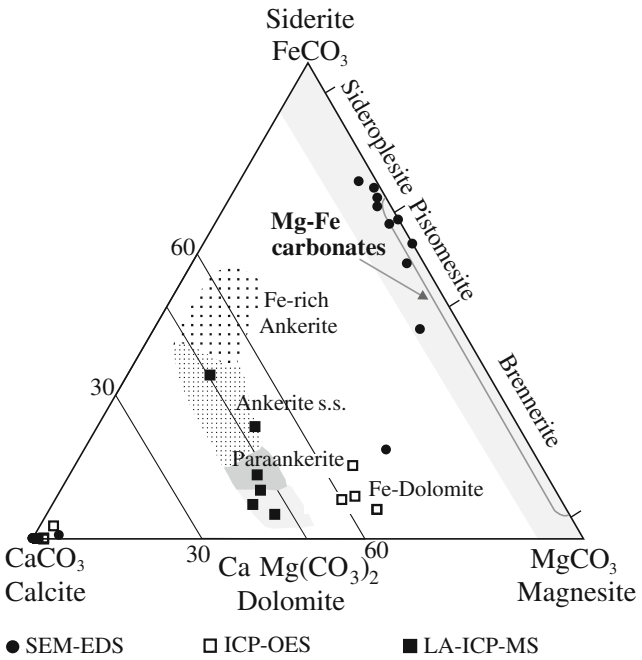

Fig. 9 Ternary plot showing compositional ranges of ore-related hydrothermal Ca-Fe-Mg carbonates from Roc Blanc Pb-Zn-Ag-Au deposit in terms of $CaCO_3$-$FeCO_3$-$MgCO_3$ components. Data from LA-ICP-MS, ICP-OES, and SEM-EDS analyses (see the text for the explanation). Classification of siderite-magnesite mineral species from Deer et al. (1962)

average, the highest concentrations, with total REY contents (ΣREY) ranging from 142 to 464 ppm (avg = 255 ppm); calcite separates have the lowest ΣREY contents (12–19 ppm; avg = 15 ppm). Similar to results for REY, Sr contents vary over a wide range from 19 to 644 ppm, with calcite separates having on average the highest concentrations (270–630 ppm). Contents of U, Th, and Ba, in contrast, are very low, commonly close to detection limits.

PAAS-normalized REY data display broadly convex-upward patterns that are depleted in light rare earth elements (LREE) and heavy rare earth elements (HREE) relative to middle rare earth elements (MREE) and Y (Fig. 11). These patterns are similar to those of metamorphic carbonates (Bau and Möller 1992; Hein 1993). An exception is sample $RB_{9–19}$ (ESM 2) that shows an increase in abundances from La to Y and little change from Y to Lu $(La/Yb)_{PAAS} = 0.1$). Overall, the patterns show variable negative to large positive Eu anomalies (Eu/Eu* 0.74–6.5), no to little Y anomalies, and no Ce anomalies.

The PAAS-normalized patterns and ΣREY contents are clearly linked to the carbonate compositions, with ΣREY increasing, and $(Sm/Yb)_{PAAS}$ decreasing, from calcite to ferroan dolomite to ankerite. Positive Eu anomalies are shown by ankerite separates only, whereby Eu*/Eu increases with increasing Fe content. Nevertheless, broad similarity among the REY patterns of the Roc Blanc ore-related Ca-Fe-Mg carbonates suggests that the parental fluids had broadly similar compositions.

LA-ICP-MS data indicate a correlation between the Eu anomaly, depth (800 m down dip of the veins), and position of the analyzed carbonate within the paragenetic sequence. Positive Eu anomalies are recorded in paragenetically early carbonate samples collected from the deepest parts of the drill holes, whereas negative Eu anomalies are restricted to shallow samples containing post-ore carbonate-3.

Carbon and oxygen isotopes

Carbon and oxygen isotope compositions for ore-related hydrothermal Ca-Fe-Mg carbonates are given in Table 2 and shown in Fig. 12. The isotopic compositions of ferroan dolomite ($n = 9$) and calcite ($n = 6$) are tightly clustered and overlap, with $\delta^{18}O_{V\text{-}SMOW}$ and $\delta^{13}C_{V\text{-}PDB}$ values of 22.6 ± 0.4‰ (1σ) and − 7.2 ± 0.4‰, respectively, for ferroan dolomite, and 20.7 ± 2.0‰ and − 7.6 ± 1.0‰ for calcite. Siderite-ankerite $\delta^{18}O$ and $\delta^{13}C$ values overlap those of ferroan dolomite and calcite, but show wider ranges with $\delta^{18}O$ and $\delta^{13}C$ values ranging from 15.7 to 23.2‰ (avg = 20.8 ± 2.8‰, $n = 8$) and − 6.1 to − 10.6‰ (avg = − 7.4 ± 1.8‰, $n = 8$), respectively.

Compared to typical marine carbonates of Carboniferous age (Veizer et al. 1999; Jenkyns et al. 2002), ore-related hydrothermal Ca-Fe-Mg carbonates of the Roc Blanc are depleted in both $\delta^{18}O$ and $\delta^{13}C$ (Fig. 12). It is noteworthy that all of the recorded $\delta^{13}C_{V\text{-}PDB}$ values for the different generations of these carbonates are negative, ranging from − 10.6 to − 5.0‰.

Strontium isotopes

Strontium isotope compositions were determined for four whole-rock samples of dominant country rocks, 1 graphite-rich black shale, 2 silty limestones and 1 rhyodacite, and for 19 ore-related hydrothermal Ca-Fe-Mg carbonate separates including 8 ferroan dolomite, 6 siderite-ankerite, and 5 calcite that span the sequence of mineral deposition (Fig. 10). The results are summarized in Table 2 and shown in Fig. 13.

The $^{87}Sr/^{86}Sr$ ratios of the ore-related siderite-ankerite separates vary from 0.714052 to 0.715961 (avg 0.714731, $n = 6$), whereas those of the ferroan dolomite vary over a wider range from 0.708043 to 0.714535 (avg 0.710989, $n = 8$). Conversely, $^{87}Sr/^{86}Sr$ ratios of the calcite separates are more homogenous, from 0.713888 to 0.716049 (avg 0.714982, $n = 5$).

All of the measured $^{87}Sr/^{86}Sr$ ratios are more radiogenic than Carboniferous and Triassic seawater values of 0.7075 to 0.7085 (Burke et al. 1982; McArthur et al. 2001) (Fig. 13). Nevertheless, the $^{87}Sr/^{86}Sr$ ratios of silty limestone (0.711108 ± 9, $n = 2$) are lower than those reported for Visean rhyodacite (0.717088 ± 7); the graphite-rich schistose black shale displays the highest $^{87}Sr/^{86}Sr$ ratios of 0.737615 ± 9.

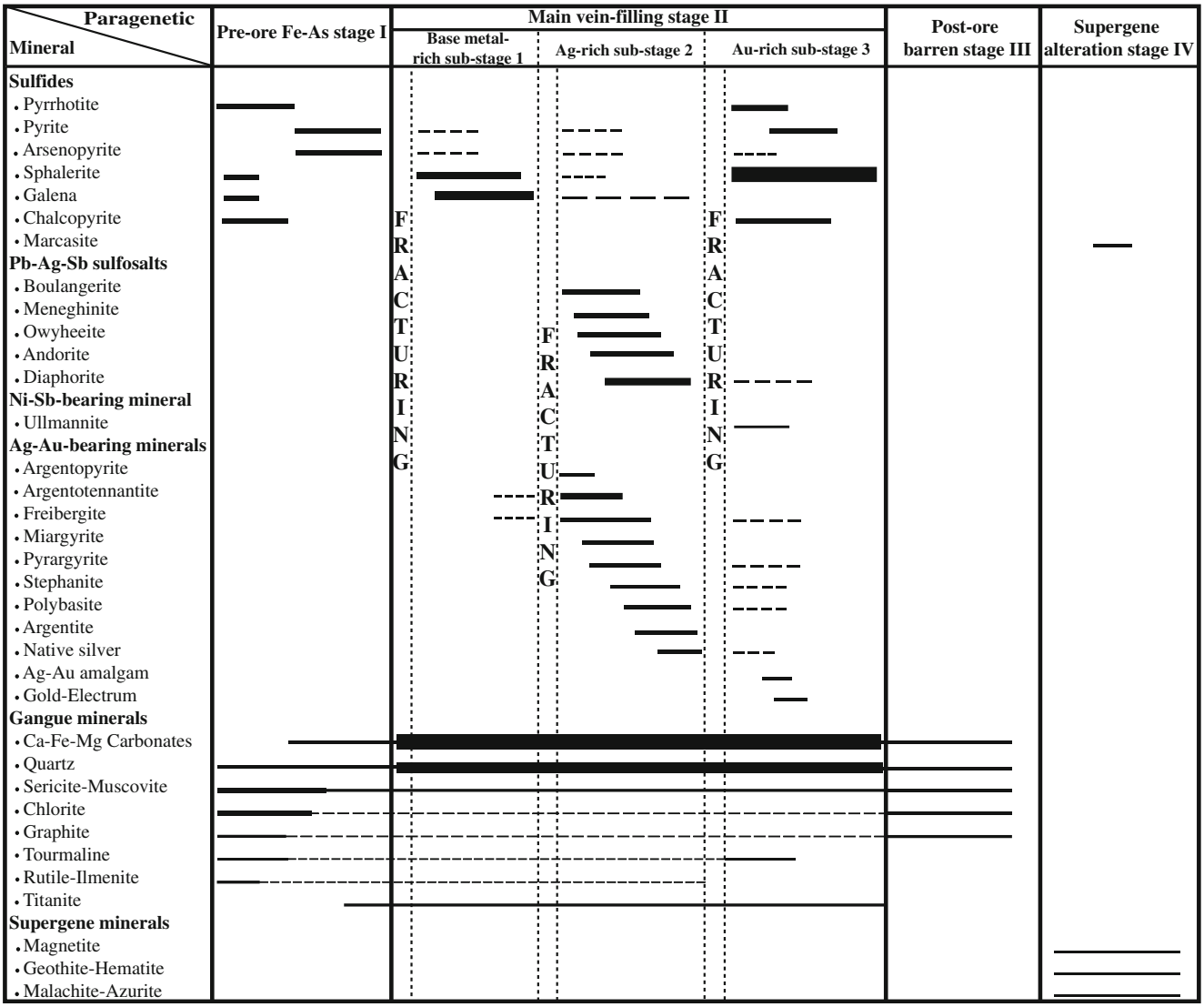

Fig. 10 Idealized paragenetic sequence of Roc Blanc Pb-Zn-Ag-Au deposit and associated alteration zones interpreted from ore textures and sulfide-sulfosalt mineral assemblages. Horizontal lines indicate relative timing of mineral formation. Line thicknesses represent, schematically, relative abundance of precipitated minerals. Dotted lines indicate uncertainties

Lead isotopes

In order to complement the Pb isotope database of Chouhaïdi (1986), 6 galena separates were analyzed for Pb isotope compositions from different mineralized veins of the Roc Blanc deposit. The existing Pb isotope data for the host rocks, mainly granite (Mrini et al. 1992) are compared with those for the Pb-rich ores, in order to (1) constrain possible source(s) of the Pb and, by inference, other accompanying metals (Zn ± Ag ± Au); (2) delineate hydrothermal fluid flow pathways; and (3) evaluate fluid-rock interactions that resulted from passage of the hydrothermal fluid.

The galena Pb isotope compositions plot in a tight linear cluster on or slightly above the Orogen Curve of Zartman and Doe (1981), showing fairly uniform $^{206}Pb/^{204}Pb$ (17.13–18.28), $^{207}Pb/^{204}Pb$ (15.87–15.63), and $^{208}Pb/^{204}Pb$ (38.20–38.31) ratios. These ratios are broadly consistent with the previously published isotope data of Chouhaïdi (1986) (Table 3; Fig. 14).

Discussion

Timing of vein emplacement

Owing to the absence of precise geochronological data for the Roc Blanc mineralization, the timing of base metals, silver, and gold relative to the succession of thermal events remains controversial (Huvelin 1977; Essarraj et al. 2017).

The maximum age for emplacement of the Pb-Zn-Ag-Au-bearing veins is constrained by cross-cutting relationships that indicate the sheared and proto-mylonitic zones and associated

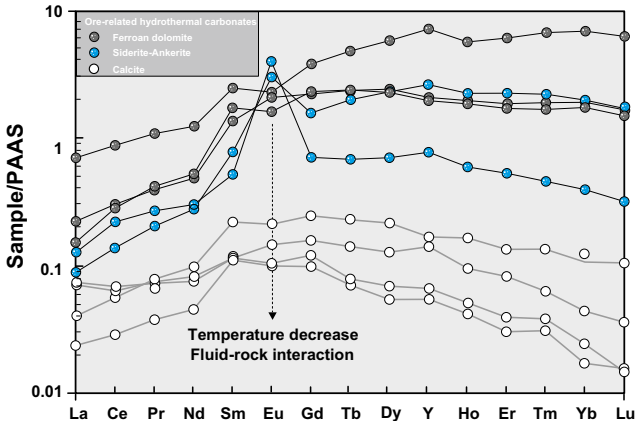

Fig. 11 Post-Archean Australian Shale (PAAS)-normalized REY plot of various generations of ore-related hydrothermal Ca-Fe-Mg carbonates from Roc Blanc Pb-Zn-Ag-Au deposit, with PAAS normalization values from McLennan (1989)

vein system truncate both the regional foliation (S_1–S_2) and the Bamega-Tabouchennt-Bramram, and Oulad Ouaslam granitic intrusions (Fig. 3). As result of these geologic constraints, the mineralization must be younger than the ca. 327 ± 4 to 295 ± 15 Ma emplacement age of the intrusions. Metamorphic-deformation relationships indicate that the bulk of the Roc Blanc mineralization occurred during the latest stage of the ductile-brittle D_2–D_3 deformation, between the early syn-D_2 transpression that outlasted emplacement of the late Variscan granitic intrusions, and the late D_3 transtension that took place during or after the peak of M_2 metamorphism dated at 315 ± 5 to 295 ± 5 Ma (Huvelin 1977; Huon et al. 1985; Michard et al. 2010). Conversely, the minimum age for the mineralization is based on the ca. 255 to 235 Ma age of microdiorite dikes (Youbi et al. 2001; Dostal et al. 2005) that cut the vein system (Fig. 4). Collectively, these relationships indicate that the Roc Blanc mineralization is bracketed between 295 and 235 Ma, coincident with the end of the latest phase of ductile-brittle deformation, during Variscan orogenic collapse.

Physico-chemical conditions and source(s) of ore fluids

Insights into probable source(s) of the mineralizing fluids that formed the Roc Blanc deposit are provided by trace element geochemistry including REYs, fluid inclusion data (Essarraj et al. 2017), and stable (C, O, H) isotopes of ore-related hydrothermal Ca-Fe-Mg carbonates. Together, the data suggest that diverse fluids were involved in the genesis and evolution of the mineralizing system.

Assuming a minimum formational temperature of 350 °C as inferred from mineral geothermometry of arsenopyrite and alteration chlorite, calculated oxygen isotope compositions of the ore-forming fluid using the dolomite-H_2O, siderite-H_2O, and calcite-H_2O fractionations of Zheng (1993, 1999), are 18.0 ± 0.4, 15.5 ± 2.8, and 16.1 ± 2.0‰, respectively (Table 2). These values are similar to those reported for fluids related to the majority of orogenic gold deposits worldwide (McCuaig and Kerrich 1998; Groves et al. 2003; Goldfarb and Groves 2015) and suggest that the ore-related hydrothermal Ca-Fe-Mg carbonates of the Roc Blanc deposit precipitated from a homogenous fluid under near-isothermal conditions. The calculated $\delta^{18}O_{fluid}$ ranges, coupled with the δD values of − 60 to − 37‰ (Essarraj et al. 2017), indicate that the mineralizing fluid originated from a metamorphic source. The low $\delta^{13}C$ values averaging − 7.1 ± 1.2‰ (Table 2) suggest an organic origin for the carbon.

Calculated Y/Ho ratios that are lower than 40 (18–38; ESM 2) are consistent with chondritic values (Y/Ho = 24–34; Bau

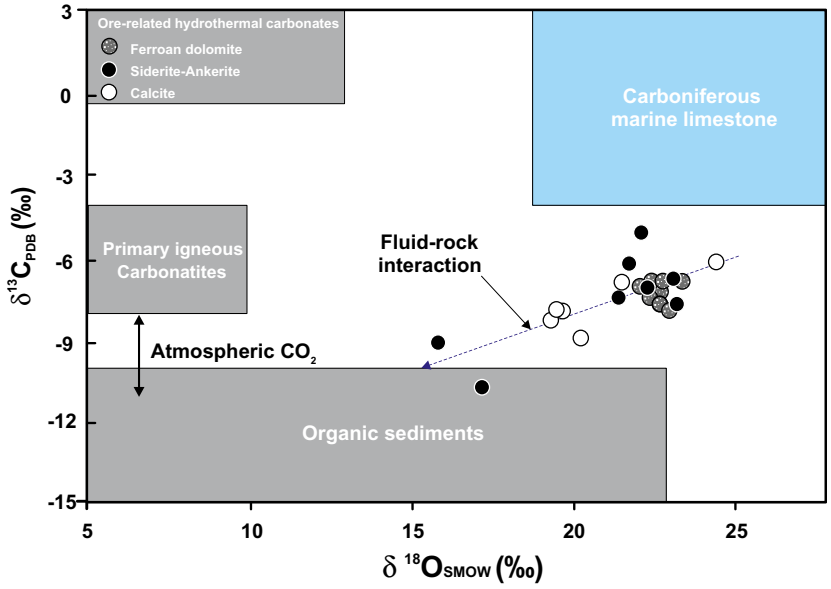

Fig. 12 Plot of $\delta^{18}O$ versus $\delta^{13}C$ compositions of ore-related hydrothermal Ca-Fe-Mg carbonates from main veins of Roc Blanc Pb-Zn-Ag-Au deposit. Compositions of Carboniferous marine limestone, primary igneous carbonatites, and organic sediments are from Jenkyns et al. (2002), Taylor et al. (1967), and Sheppard (1986); respectively

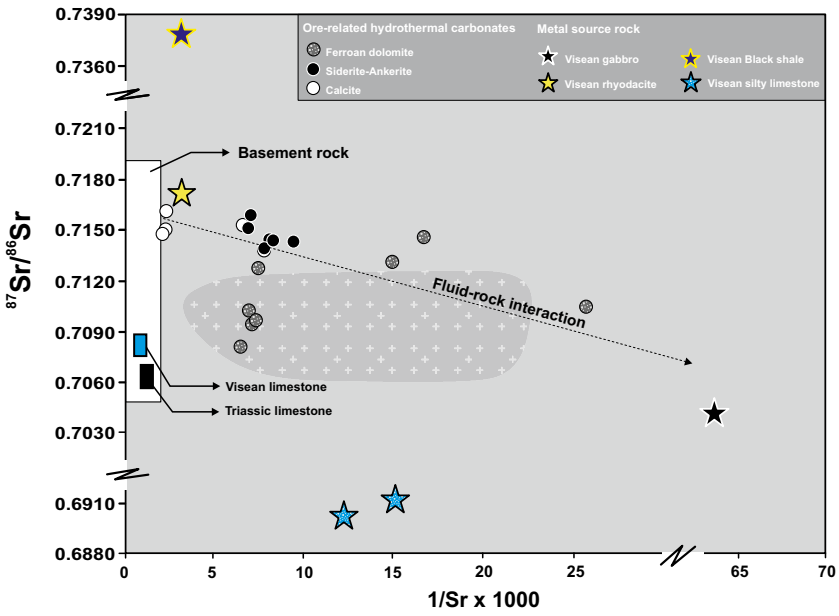

Fig. 13 Plot of $^{87}Sr/^{86}Sr$ versus 1/Sr showing isotopic compositions of various generations of ore-related Ca-Fe-Mg hydrothermal carbonates from Roc Blanc Pb-Zn-Ag-Au deposit compared to those of potential metal sources (i.e., organic-rich black shale, rhyodacite, late Variscan granite). Granitoid compositional field is drawn based on data from Mrini et al. (1992)

1991) but are incompatible with entrainment of seawater into the hydrothermal system as proposed by Essarraj (2017). A marine sedimentary origin for the carbon is ruled out, because in this model the resulting $\delta^{13}C$ value would be close to 0‰ (Deines 2002). Influx of surface-derived meteoric water during regional uplift also seems unlikely because a concomitant lowering of the $\delta^{18}O$ values is expected in this case.

Collectively, the stable isotope data indicate that the composition of the mineralizing fluid is restricted to metamorphic sources. These fluids may have been produced during emplacement of late Variscan granitic intrusions and devolatilization of associated graphite-rich black shales.

Controls on fluid flow, fluid-rock interaction, and metal sources

Elevated REY contents of ore-related hydrothermal Ca-Fe-Mg carbonates, particularly siderite-ankerite and ferroan dolomite from the main vein filling stage II, suggest that the hydrothermal fluids interacted with graphite-rich black shale in the crust or with spatially associated Late Variscan granitoids.

Table 3 Lead isotope compositions of galena from Roc Blanc Pb-Zn-Ag-Au deposit

Sample no.	$^{206}Pb/^{204}Pb$	$^{207}Pb/^{204}Pb$	$^{208}Pb/^{204}Pb$
RB 22	18.2515	15.5958	38.2024
RB 23	18.2743	15.6221	38.2479
RB 25	18.2718	15.6253	38.2637
RB 27	18.2832	15.6351	38.2956
RB 31	18.2872	15.6336	38.3147
RB 32	17.1340	14.87089	36.3013

The depletion in LREE relative to HREE of the hydrothermal Ca-Fe-Mg carbonates (Fig. 11) provides further evidence for intensive fluid-rock interaction owing to enhanced solubility of LREE over HREE complexes (Wood 1990; Bau and Möller 1992). Notably, the positive Eu_{PAAS} anomaly shown by ankerite (Fig. 11) is consistent with Eu^{2+} being derived from the breakdown of feldspar in the spatially associated Late Variscan granitoids, followed by precipitation from reduced high-temperature (> 250 °C) hydrothermal fluids (Bau and Möller 1992).

Close similarity of the Sr isotopic compositions of ore-related siderite-ankerite and calcite, and partial overlap between the compositions of ferroan dolomite and siderite-ankerite and calcite, suggests that the mineralizing fluids had a common source of Sr. Visean silty limestones are excluded as a potential source because of their lower Sr isotopic ratios (0.710535–0.711681) at the time of deposition compared to the ore-related Ca-Fe-Mg carbonates (0.708043–0.716049). The overall tendency for the Sr isotope compositions to define a linear array, for which end-members are broadly defined by the radiogenic graphitic black shale and the late Variscan granitic intrusions, implies a mixed source for the Sr and, by inference, for water-rock exchange. Assuming the above-mentioned lithotypes as end-members (graphitic black shale, Sr = 150 ppm and $^{87}Sr/^{86}Sr = 0.718$; granitoids, Sr = 350 ppm, and $^{87}Sr/^{86}Sr = 0.707$), mass-balance calculations using the equation of Castorina and Masi (2000) suggest a contribution of about 20–25% of Sr from the late Variscan granitic rocks, consistent with the Pb isotope data (Fig. 14). The overlap between Pb isotope compositions of the K-feldspar from the Tabouchennt-Bramram granodiorite and those of galena

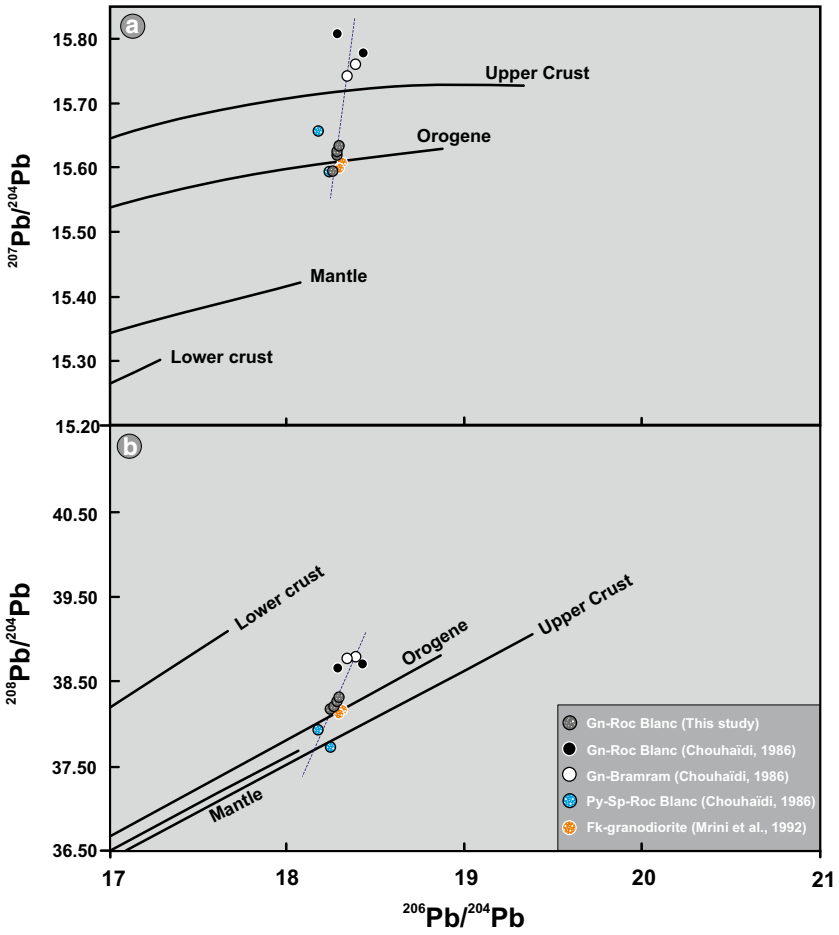

Fig. 14 Lead isotopic compositions of galena from Roc Blanc Pb-Zn-Ag-Au deposit plotted on **a** $^{208}Pb/^{204}Pb$ vs $^{206}Pb/^{204}Pb$ and **b** $^{207}Pb/^{204}Pb$ vs $^{206}Pb/^{204}Pb$ diagrams. Also shown are K-feldspar data of Mrini et al. (1992). Evolution curves are from Zartman and Doe (1981)

implies that the late Variscan granitic intrusions were the main Pb source in the Roc Blanc deposit.

Taking into consideration all of these constraints, we suggest that the graphitic black shale and Late Variscan intrusions were the major source-rock reservoirs for metals to the Roc Blanc ore fluids, in which all contributed metals were leached by metamorphic fluids, as discussed above.

Fluid immiscibility vs fluid mixing

Variations in the hydrogen isotope composition in excess of 25‰, as shown by the range of δD values between − 60 and − 37‰ (Essarraj et al. 2017), could be produced by fluid immiscibility (Kerrich 1987; Taylor 1997), and by changes in the oxygen fugacity of the fluid at the depositional sites due to hydrogen isotope fractionation between water and reduced species such as CH_4 and/or H_2 (Colvine et al. 1988; Klein et al. 2006). Fluid unmixing could occur during pressure-driven migration of the hydrothermal fluid in the transition from ductile to brittle regime as suggested by structural constraints. In this regard, it is well established that fluids having significant fractions of both water and nonpolar species (CO_2, CH_4, or N_2) may display fluid immiscibility under metamorphic conditions (Yardley and Bottrell 1988).

The uniformity in $\delta^{13}C$ values together with calculated $\delta^{18}O_{fluid}$ values of the ore-related hydrothermal Ca-Fe-Mg carbonates (Table 3), plus the lack of correlation between final homogenization temperatures and salinity (Essarraj et al. 2017), preclude fluid mixing as a major depositional process.

Fluid cooling vs fluid-rock interaction

Although the Roc Blanc ore-related hydrothermal Ca-Fe-Mg carbonates show variable degrees of REY enrichment, shapes of the PAAS-normalized patterns are broadly similar (Fig. 11) suggesting a common fluid source. A noteworthy feature of these patterns is a change from positive to negative Eu anomalies towards the surface and younger carbonate generations.

Positive Eu anomalies are thought to develop mainly in reduced, high-temperature (> 250 °C) hydrothermal systems, whereas negative Eu anomalies occur in lower temperature (< 200 °C) systems (Bau and Möller 1992; Sverjensky 1984). The switch from positive to negative Eu anomalies is consistent with either a temperature decrease or a change in Eh from reducing to oxidizing conditions. A temperature decrease is unlikely considering the constant $\delta^{18}O_{fluid}$ values. Alternatively, the well-developed hydrothermal alteration zones present on both sides of the Pb-Zn-Ag-Au veins,

together with REY and isotopic constraints discussed above, provide key evidence that fluid-rock interaction along the fluid pathway played a crucial role in the evolution of the hydrothermal fluid.

The isotopic trend of $\delta^{13}C$-$\delta^{18}O$ values shown in Fig. 12 suggests that metamorphic fluids interacted with the graphitic black shale host rock and Late Variscan intrusions during fluid migration. Further support for this fluid-rock mechanism is provided by (1) depletion of ore-related hydrothermal carbonates in LREE relative to HREE (Fig. 11), because LREE are generally more mobile than HREE; (2) the presence of large amounts of nonpolar species such as CO_2, CH_4 and N_2 in the mineralizing fluid (Bastoul 1992); and (3) involvement of the country rocks as metal sources. Collectively, the above evidence supports the fluid flow model involving deep circulation of metamorphic fluids that interacted extensively with enclosing host rocks along the Marrakech Shear Zone and associated subsidiary strike-slip faults. Although water/rock ratios cannot be quantified, the reactions occurred in a fluid-dominated system under nearly isothermal conditions as suggested by the low variance in fluid isotope compositions of ore-related hydrothermal Ca-Fe-Mg carbonates.

Classification of the Roc Blanc deposit

By combining field observations with mineral chemistry and isotope geochemistry, it is apparent that the Roc Blanc deposit shares characteristics that are analogous to those of orogenic gold deposits hosted in metamorphic terranes (Groves et al. 2000; Goldfarb et al. 2001; Goldfarb and Groves 2015). These characteristics include (1) polyphase deformed and low- to medium-grade metamorphosed host rocks; (2) wall-rock alteration and mineral assemblages dominated by sulfides and sulfosalts in a gangue of quartz, carbonates, sericite-muscovite, chlorite, and tourmaline; (3) strong structural control on lead-zinc-silver-gold mineralization with the resulting orebodies being hosted by the brittle-ductile mylonitic Marrakech Shear Zone and related subsidiary brittle structures; (4) late orogenic timing with Ag-Au-bearing mineralization having formed during or shortly after regional peak deformation and associated greenschist- to amphibolite-facies metamorphism, during a time period characterized by a switch from a transpressional to transtensional deformation regime; and (5) an Au-Ag-As-Sb metal enrichment. Permissive features include the "orogenic" trace element signature of ore-related pyrite (Fig. 8) and the widespread development of graphite along the shear structures. The unusual base metal sulfide-rich nature of the Roc Blanc ores may reflect different physico-chemical conditions (fugacities of oxygen and sulfur) during mineralization.

In summary, we propose that the Roc Blanc Pb-Zn-Ag-Au mineralization belongs to the class of orogenic mineral deposits. As such, this is the first polymetallic deposit of orogenic affiliation defined in the North African Variscides. A comparison of the Roc Blanc deposit with equivalent late Variscan gold-bearing deposits of Western Europe (Bellot et al. 2003 and references herein) reveals a number of similarities, which can be attributed to regional-scale, rather than local, processes related to plate-tectonic reorganization of the stress field at ca. 300 Ma, as a result of convergence of the Gondwanan and Laurussian supercontinents.

Concluding remarks: a fluid-structural genetic model

Our study documents the occurrence of late-stage gold mineralization that underpins a new genetic model for the Roc Blanc Pb-Zn-Ag-Au deposit. The new model, centered on structural control by the ductile-brittle Marrakech Shear Zone, involves a transtensional, syn- to late orogenic (D_2–D_3 to late D_3) mineralizing event associated with pervasive alteration (quartz, muscovite, chlorite, carbonate, and sulfide), veining and fracturing, and upward flow of deeply sourced metamorphic fluids along this shear zone.

Relative timing constrains emplacement of the Roc Blanc mineralization between 295 and 235 Ma following the peak of greenschist- to amphibolite-facies metamorphism at 290 ± 4 Ma (Huon 1985; Huon et al. 1988). From a geodynamic point of view, this time interval coincides with waning stages of the Variscan orogeny characterized by prolonged plate convergence between Gondawana and Laurussia and concomitant plate-tectonic reorganization of the stress field at ca. 300 Ma.

Integrated structural, mineralogical, fluid inclusion, and stable and radiogenic isotope data suggest that deposition of the Roc Blanc polymetallic quartz-carbonate veins took place within dilatational faults. Geodynamically, development of these extensional faults is thought to have occurred during the late Carbonifeous-Early Permian following closure of the Rheic Ocean, driven by an easterly subduction zone (Simancas et al. 2005, 2009; Michard et al. 2010) in response to the collision between Gondwana and Laurussia that formed Pangea–North Africa.

Mineral geothermometry of arsenopyrite and alteration chlorite indicate hydrothermal temperatures of 330 to 370 and 352 to 382 °C, respectively, similar to the temperature ranges at which most orogenic gold deposits formed (Goldfarb and Groves 2015). The P-T trapping conditions of fluid inclusions in the Roc Blanc deposit yield an estimated pressure range of 200 ± 20 MPa (Bastoul 1992) to 50 MPa (Essarraj et al. 2017) corresponding to depths of 8 to 2 km (mesozonal to epizonal), respectively.

Recognized types of hydrothermal alteration of the host rocks include silicification, sericitization, chloritization, carbonatization, and sulfidation. The ranges of calculated

$\delta^{18}O_{fluid}$ values (15.5–18.0‰) and δD values (− 60 to − 37‰; Essarraj et al. 2017) are consistent with upward migration of deep-seated metamorphic fluids sourced from the Late Variscan granitoids and decarbonation and dehydration reactions, perhaps coeval with emplacement of the intrusions within the Visean organic-rich host rocks. Ore deposition occurred in response to complex and concurrent processes involving metamorphic fluid immiscibility and fluid-rock interaction. Fluid mixing and dilution as possible triggers to Pb-Zn-Ag-Au mineralization seem unlikely. Sulfur and base, precious, and trace metals are thought to have been sourced through fluid-rock interactions between the upward migrating mineralizing fluids and host rocks at depth.

Acknowledgements The authors are grateful to Managem Group geologists, in particular Mohamed Zouhair, Abdelmalek Ouadjou, and Ahmed Radnaoui, for the technical and logistical support during the field work. Stefano Poli and Andrea Risplendente from the University of Milano (Italy) are thanked for electron microprobe analyses and D. Margoum for the help in the preparation of the figures. Special appreciation is extended to Rich Goldfarb who was very generous in providing valuable insights and careful editing of an early version of the manuscript. We are also deeply grateful to J.F. Slack and D. Gasquet for their fruitful and constructive comments and to Associate Editor P. Eilu and Editor G. Beaudoin for the careful handling, all of which improved this manuscript substantially.

References

Barton PB Jr (1978) Some ore textures involving sphalerite from the Furutobe mine, Akita Prefecture, Japan. Mining Geol 28:293–300

Barton PB Jr, Skinner BJ (1979) Sulfide mineral stabilities. In: Barnes HL (ed) Geochemistry of hydrothermal ore deposits, 2nd edn. Wiley, New York, pp 278–403

Barton PB Jr, Bethke PM (1987) Chalcopyrite disease in sphalerite: pathology and epidemiology. Am Mineral 72:451–467

Bastoul A (1992) Origin and evolution of C-H-O-N fluids in the metamorphic formations: relations with the associated mineralisations (U, Au, graphite). Unpubl PhD thesis, Université de Nancy 1, Nancy, France, 311 pp

Bau M (1991) Rare-earth element mobility during hydrothermal and metamorphic fluid-rock interaction and the significance of the oxidation state of europium. Chem Geol 93:219–230

Bau M, Möller P (1992) Rare earth element fractionation in metamorphogenic hydrothermal calcite, magnesite and siderite. Mineral Petrol 45:231–246

Bellot J-P, Lerouge C, Bailly L, Bouchot V (2003) The Biards Sb-Au–bearing shear zone (Massif Central, France): an indicator of crustal-scale transcurrent tectonics guiding late Variscan collapse. Econ Geol 98:1427–1447

Boiron MC, Cathelineau M, Dubessy J, Bastoul AM (1990) Fluids in Hercynian Au veins from the French Variscan belt. Min Mag 54: 231–243

Boiron MC, Cathelineau M, Banks DA, Fourcade S, Vallance J (2003) Mixing of metamorphic and surficial fluids during the uplift of the Hercynian upper crust: consequences for gold deposition. Chem Geol 194:119–141

Bordonaro M (1983) Tectonique et pétrographie du district à pyrrhotite de Kettara (Paléozoïque des Jebilet, Maroc). Unpublished PhD thesis, Université Louis Pasteur, Strasbourg, France, 132 pp

Bordonaro M, Gaillet JL, Michard A (1979) Le géosynclinal carbonifère sud-mésétien dans les Jebilet (Maroc); une corrélation avec la province pyriteuse du sud de l'Espagne. Comptes Rendus Acad Sci Paris Sér D 288:1371–1374

Bouabdellah M, Niedermann S, Velasco F (2015) The Touissit-Bou Beker Mississippi Valley-type district of northeastern Morocco: relationships to the Messinian salinity crisis, Late Neogene-Quaternary alkaline magmatism, and buoyancy-driven fluid convection. Econ Geol 110:1455–1484

Bouabdellah M, Slack JF (2016) Geologic and metallogenic framework of North Africa. In: Bouabdellah M, Slack JF (eds) Mineral deposits of North Africa. Springer-Verlag, Mineral Resource Reviews, Berlin-Heidelberg, pp 3–81

Bouloton J (1992) Mise en évidence de cordiérite héritée des terrains traversés dans le pluton granitique des Oulad Ouaslam (Jebilet, Maroc). Can J Earth Sci 29:658–668

Boummane MH, Olivier PH (2007) The Oulad Ouaslam Variscan granitic pluton (Jebilet massif, southwestern Moroccan Meseta): a forcibly emplaced laccolithic intrusion characterized by its magnetic and magmatic fabrics. J Afr Earth Sci 47:49–61

Burke WH, Denison RE, Hetherington EA, Koepnick RB, Nelson HF, Otto JB (1982) Variation of seawater $^{87}Sr/^{86}Sr$ throughout Phanerozoic time. Geology 10:516–519

Burrows DR, Wood PC, Spooner ETC (1986) Carbon isotope evidence for a magmatic origin for Archean gold-quartz vein ore deposits. Nature 321:851–854

Castorina F, Masi U (2000) Sr-isotopic composition of siderite for assessing the origin of mineralizing fluid: the case study from the Jebel Awam deposit (Central Morocco). Ore Geol Rev 17:83–89

Cathelineau M, Nieva D (1985) A chlorite solid solution geothermometer the Los Azufres (Mexico) geothermal system. Contrib Mineral Petrol 91:235–244

Chouhaïdi MY (1986) Contribution a l'étude pétrographique, géochimique et métallogénique des minéralisations argentifères des Jebilet centrales (l'exemple de Roc Blanc). Unpub PhD thesis, Université de Nancy, Nancy, France, 282 pp

Colvine AC, Fyon JA, Heather KB, Marmont S, Smith PM, Troop DG (1988) Archean lode gold deposits in Ontario. Ontario Geological Survey Miscellaneous Paper 139:136

Conliffe J, Wilton DHC, Blamey NJF, Archibald SM (2013) Paleoproterozoic Mississippi Valley type Pb–Zn mineralization in the Ramah Group, northern Labrador: stable isotope, fluid inclusion and quantitative fluid inclusion gas analyses. Chem Geol 362:211–223

Deditius AP, Reich M, Kesler SE, Utsunomiya S, Chryssoulis SL, Walshe J, Ewing RC (2014) The coupled geochemistry of Au and As in pyrite from hydrothermal ore deposits. Geochim Cosmochim Acta 140:644–670

Deer WA, Howie RA, Zussman J (1962) Rock forming minerals: non silicates: Logmans, London, 5, 371 pp

Deines P (2002) The carbon isotope geochemistry of mantle xenoliths. Earth-Sci Rev 50:247–278

Delchini S, Lahfid A, Plunder A, Michard A (2016) Applicability of the RSCM geothermometry approach in a complex tectono-metamorphic context: the Jebilet massif case study (Variscan belt, Morocco). Lithos 256–257:1–12

Dostal J, Keppie JD, Hamilton MA, Aarab EM, Lefort JP, Murphy JB (2005) Crustal xenoliths in Triassic lamprophyre dykes in western Morocco: tectonic implications for the Rheic Ocean suture. Geol Mag 142:159–172

Dubé B, Gosselin P (2007) Greenstone-hosted quartz-carbonate vein deposits. In: Goodfellow WD (ed) Mineral deposits of Canada: a synthesis of major deposit types, district metallogeny, the evolution of geological provinces, and exploration methods. Geol Assoc Canada, Min Deposits Div, Spec Publ 5, pp 49–74

El Hassani A, Zahraoui M (1982) Evolution tectono-métamorphique des unités structurales du segment hercynien des Jebilet centrales. Bulletin Institut Scientifique Rabat 6:45–51

Essaifi A, Lagarde JL, Capdevila R (2001) Deformation and displacement from shear zone patterns in the Variscan upper crust, Jebilet, Morocco. J Afr Earth Sci 32:335–350

Essaifi A, Samson S, Goodenough K (2014) Geochemical and Sr–Nd isotopic constraints on the petrogenesis and geodynamic significance of the Jebilet magmatism (Variscan belt, Morocco). Geol Mag 151:666–691

Essarraj S, Boiron MC, Cathelineau M, Tarantola A, Leisen M, Hibti M (2017) Mineralogy and ore fluid chemistry of the Roc Blanc Ag deposit, Jebilet Hercynian massif, Morocco. J Afr Earth Sci 127: 175–193

Gasquet D, Bouloton J (1995) Les filons de microdiorite des Jebilets centrales (Meseta marocaine): pré-rifting permien? Réunion extraordinaire SGF, Marrakech, abstract, pp. 55

Gasquet D, Stussi JM, Nachit H (1996) Les granitoïdes hercyniens du Maroc dans le cadre de l'évolution géodynamique régionale. Bull Soc Géol Fr 167-4:517–528

Goldfarb RJ, Groves DI (2015) Orogenic gold: common or evolving fluid and metal sources through time. Lithos 233:2–26

Goldfarb RJ, Groves DI, Gardoll S (2001) Orogenic gold and geologic time: a global synthesis. Ore Geol Rev 18:1–75

Goldfarb RJ, Baker T, Dubé B, Groves DI, Hart CJ, Gosselin P (2005) Distribution, character and genesis of gold deposits in metamorphic terranes. In: Hedenquist JW, Thompson JFH, Goldfarb RJ, Richards JP (eds) Econ Geol 100th Anniv Vol, pp. 407–450

Groves DI, Phillips GN (1987) The genesis and tectonic control on Archaean gold deposits of the western Australian shield—a metamorphic replacement model. Ore Geol Rev 2:287–322

Groves DI, Goldfarb RJ, Gebre-Mariam M, Hagemann SG, Robert F (1998) Orogenic gold deposits: a proposed classification in the context of their crustal distribution and relationship to other gold deposit types. Ore Geol Rev 13:7–27

Groves DI, Goldfarb RJ, Knox-Robinson CM, Ojala J, Gardoll S, Yun G, Holyland P (2000) Late-kinematic timing of orogenic gold deposits and significance for computer-based exploration techniques with emphasis on the Yilgarn block, Western Australia. Ore Geol Rev 17:1–38

Groves DI, Goldfarb RJ, Robert F, Hart CJ (2003) Gold deposits in metamorphic belts: overview of current understanding, outstanding problems, future research, and exploration significance. Econ Geol 98:1–29

Hagemann SG, Gebre-Mariam G, Groves DI (1994) Surface water influx in shallow level Archean lode gold deposits in Western Australia. Geology 22:1067–1070

Hein UF (1993) Synmetamorphic Variscan siderite mineralization of the Rhenish massif, Central Europe. Min Mag 57:451–467

Hey MH (1954) A new review of the chlorites. Min Mag 30:277–292

Huon S, Piqué A, Clauer N (1985) Etude de l'orogenèse hercynienne au Maroc par la datation K-Ar de l'évolution des schistes ardoisiers. Sci Géol Bull 40:273–284

Huon S, Kfibler B, Hunziker J (1988) Identification de mélanges de micas blancs par diffraction des rayons X: application à des séries carbonatées faiblement métamorphisées. Schweiz Mineral Petrogr Mitt 68:185–202

Huvelin P (1977) Etude géologique et gîtologique du Massif hercynien des Jebilet (Maroc occidental). Notes Mémoires Service Géologique Maroc 232bis:1–307

Huvelin P, Moelo Y, Permingeat F, Picot P (1978) Sur la minéralisation du champ filonien polymétallifère du Roc Blanc (Jebilet centrales, Maroc). Notes Mémoires Service Géologique Maroc 40(275):239–248

Jenkyns HC, Jones CE, Gröcke DR, Hesselbo SP, Parkinson DN (2002) Chemostratigraphy of the Jurassic system: applications, limitations and implications for palaeoceanography. J Geol Soc 159:351–378

JICA [Japan International Cooperation Agency] (2003) Report on the mineral exploration in Marrakech-Tekna area: Kingdom of Morocco. Phase 1. Japan Inter Coop Agency, 247 pp

Jochum KP, Scholz D, Stoll B, Weis U, Wilson SA, Yang Q, Schwalb A, Börner N, Jacob DE, Andreae MO (2012) Accurate trace element analysis of speleothems and biogenic calcium carbonates by LA-ICP-MS. Chem Geol 318-319:31–44

Kerrich R (1987) The stable isotope geochemistry of Au-Ag vein deposits in metamorphic rocks. In: Kyser TK (ed) Stable isotope geochemistry of low temperature fluids. Mineral Association Canada Short Course 13:287–336

Klein EL, Harris C, Renac C, Giret A, Moura CAV, Fuzikawa K (2006) Fluid inclusion and stable isotope (O, H, C, and S) constraints on the genesis of the Serrinha gold deposit, Gurupi belt, northern Brazil. Mineral Deposita 41:160–178

Kranidiotis P, MacLean WH (1987) Systematics of chlorite alteration at the Phelps Dodge massive sulfide deposit, Matagami, Quebec. Econ Geol 82:1898–1911

Lagarde JL, Choukroune P (1982) Cisaillement ductile et granitoïdes syntectoniques: l'exemple du massif hercynien des Jebilet (Maroc). Bull Soc Géol Fr 24:299–307

Lagarde JL, Omar A, Roddaz B (1990) Structural characteristics of granitic plutons emplaced during weak regional deformation: examples from late Carboniferous plutons, Morocco. J Struct Geol 12:805–821

Le Corre C, Bouloton J (1987) Un modèle de "structure en fleur" associant décrochement et convergence: les Jebilet centro-occidentales (Maroc Hercynien). Comptes Rendus Acad Sci Paris Série II 13:751–755

Le Corre C, Saquaque A (1987) Comportement d'un système pluton-encaissant dans un champ de déformation régional: le granite de Bramram (Jebilet, Maroc hercynien). Bull Soc Géol Fr 4:665–673

Margoum D, Bouabdellah M, Klügel A, Banks D, Castorina F, Cuney M, Jébrak M, Bozkaya G (2015) Pangea rifting and onward pre-Central Atlantic opening as the main ore-forming processes for the genesis of the Aouli REE-rich fluorite–barite vein system, upper Moulouya district, Morocco. J Afr Earth Sci 108:22–39

Marignac C, Cuney M (1999) Ore deposits of the French Massif Central: insight into the metallogenesis of the Variscan collision belt. Mineral Deposita 34:472–504

Mayol S, Muller J (1985) Mise en évidence d'une unité allochtone hercynienne précoce (antéschisteuse) dans les Jebilet occidentales (Maroc). Etude de structuration de la zone de contact. CR Acad Sci Paris 300:369–372

McArthur JM, Howarth RJ, Bailey TR (2001) Strontium isotope stratigraphy: LOWESS version 3: best fit to the marine Sr-isotope curve for 0–509 Ma and accompanying look-up table for deriving numerical age. J Geol 109:155–170

McCuaig TC, Kerrich R (1998) P–T–t-deformation-fluid characteristics of lode gold deposits: evidence from alteration systematics. Ore Geol Rev 12:381–453

McLennan SM (1989) Rare earth elements in sedimentary rocks: influence of provenance and sedimentary processes. In: Lipin BR, McKay GA (eds) Rare earth elements. Rev Mineral 21, pp 169–200

Michard A, Soulaimani A, Hoepffner C, Ouanaimi H, Baidder L, Rjimati EC, Saddiqi O (2010) The south-western branch of the Variscan belt: evidence from Morocco. Tectonophys 492:1–24

Morelli RM, Creaser R, Selby D, Kontak DJ, Horne RJ (2005) Rhenium-osmium geochronology of arsenopyrite in Meguma Group gold deposits, Meguma terrane, Nova Scotia, Canada: evidence for multiple gold-mineralizing events. Econ Geol 100:1229–1242

Moreno C, Sáez R, González F, Almodóvar G, Toscano M, Playford G, Alansari A, Rziki S, Bajddi A (2008) Age and depositional

environment of the Draa Sfar massive sulfide deposit, Morocco. Mineral Deposita 43:891–911

Moritz R, Malo M (1996) Lead isotope signatures of Devonian Acadian structurally controlled ore occurrences in Gaspé Peninsula, Québec Appalachians: constraints on source rock reservoirs. Econ Geol 91: 1145–1150

Mrini Z, Rafi A, Duthou JL, Vidal P (1992) Chronologie Rb-Sr des granitoïdes hercyniens du Maroc: conséquences. Bull Soc Géol Fr 163:281–291

Nesbitt BE, Muehlenbachs K (1995) Geochemical studies of the origins and effects of synorogenic crustal fluids in the southern Omineca belt of British Columbia. Geol Soc Am Bull 107:1033–1050

Piqué A, Michard A (1989) Moroccan Hercynides. A synopsis. The Palaeozoic sedimentary and tectonic evolution at the northern margin of West Africa. Am Jour Sci 29:286–330

Piqué A, O'Brien S, King AF, Schenk PE, Skehan JW, Hon R (1990) La marge nord occidentale du Paléo-Gondwana (Maroc occidental et zones orientales des Appalaches): rifting au Précambrien terminal et au Paléozoïque inférieur, et compression hercynienne et alléghanienne au Paléozoïque supérieur. Comptes Rendus Acad Sci Paris Sér II 310(4):411–416

Phillips GN, Groves DI, Kerrich R (1996) Factors in the formation of the giant Kalgoorlie gold deposit. Ore Geol Rev 10:265–317

Playford G, Gonzalez F, Moreno C, Al Ansari A (2008) Palynostratigraphy of the Sarhlef series (Mississippian), Jebilet massif, Morocco. Micropaleo 54:89–124

Pokrovski GS, Kara S, Roux J (2002) Stability and solubility of arsenopyrite, FeAsS, in crustal fluids. Geochim Cosmochim Acta 66: 2361–2378

Schulmann K, Lexa O, Štípská P, Racek M, Tajčmanová L, Konopásek J, Lehmann J (2008) Vertical extrusion and horizontal channel flow of orogenic lower crust: key exhumation mechanisms in large hot orogens? J Metamorph Geol 26:273–297

Sessa G, Moroni M, Tumiati S, Caruso S, Fiorentini ML (2017) Ni-Fe-Cu-PGE ore deposition driven by metasomatic fluids and melt-rock reactions in the deep crust: the ultramafic pipe of Valmaggia, Ivrea-Verbano, Italy. Ore Geol Rev 90:485–509

Sheppard SMF (1986) Characterization and isotopic variations in natural waters. In: Valley JW, Taylor HP Jr, O'Neil JR (eds) Stable isotopes in high temperature geological processes. Mineral Soc Am Rev Mineral 16:165–184

Simancas JF, Tahiri A, Azor A, González-Lodeiro F, Martinez Poyatos DJ, El Hadi H (2005) The tectonic frame of the Variscan–Alleghanian orogen in southern Europe and northern Africa. Tectonophys 398:181–198

Simancas JF, Azor A, Martínez Poyatos DJ, Tahiri A, El Hadi H, González-Lodeiro F, Pérez-Estaún A, Carbonell R (2009) Tectonic relationships of Southwest Iberia with the allochthons of Northwest Iberia and the Moroccan Variscides. Compt Rendus Geosci 341: 103–113

Sverjensky DA (1984) Europium redox equilibria in aqueous solutions. Earth Planet Sci Lett 67:70–78

Taylor HP, Frechen J, Degens ET (1967) Oxygen and carbon isotopic studies of carbonatites from the Laacher See District, West Germany and the Alno District, Sweden. Geochim Cosmochim Acta 31:407–430

Taylor HP (1997) Oxygen and hydrogen isotope relationships in hydrothermal mineral deposits. In: Barnes HL (ed) Geochemistry of hydrothermal ore deposits, 3rd edn. Wiley, New York, pp 229–302

Tisserant D (1977) Les isotopes du strontium et l'histoire hercynienne du Maroc, Étude de quelques massifs atlasiques et mésétiens. Unpub PhD Thesis, Université Louis Pasteur, Strasbourg, France, 103 pp

Veizer J, Ala D, Azmy K, Bruckschen P, Buhl D, Bruhn F, Jasper T (1999) $^{87}Sr/^{86}Sr$, $\delta^{13}C$ and $\delta^{18}O$ evolution of Phanerozoic seawater. Chem Geol 161:59–88

Wood SA (1990) The aqueous geochemistry of the rare-earth elements and yttrium: 2. Theoretical predictions of speciation in hydrothermal solutions to 350°C at saturation water vapor pressure. Chem Geol 88:99–125

Yardley BWD, Bottrell SH (1988) Immiscible fluids in metamorphism: implications of two-phase flow for reaction history. Geology 16: 199–202

Youbi N, Bellon H, Marzin A, Piqué A, Cotten J, Cabanis B (2001) Du cycle orogénique hercynien au pré-rifting de l'Atlantique central au Maroc occidental: les microdiorites des Jbilet sont-elles des marqueurs magmatiques de ce passage. Comptes Rendus Acad Sci Paris Sér IIA 333:295–302

Zartman RE, Doe BR (1981) Plumbotectonics, the model. Tectonophys 75:135–162

Zheng YF (1993) Calculation of oxygen isotope fractionation in anhydrous silicate minerals. Geochim Cosmochim Acta 57:1079–1091

Zheng YF (1999) Oxygen isotope fractionation in carbonate and sulfate minerals. Geochem J 33:109–126